

6. Convection: Why can't we predict rainfall?

The tropical atmosphere is heated strongly at the bottom (more exactly speaking during daytime; although the daytime insolation is larger than day and night infrared cooling, the net overheating is much weaker than daytime heating and is almost zero as shown later in Fig. 6.3(a)). In such a fluid heated at the bottom in the presence of gravity may have so-called convective instability, and the result is in general relatively small-scale convection of which the horizontal scale is similar to the vertical scale, that is the order of 10 km (Section 6.2). In addition even the tropical atmosphere is rather stable without latent heating by the moist process. This involves a paradox that convection is generated by cloud, whereas cloud is generated by convection. Therefore, we shall consider at first a stable (horizontally forced) convection between sea and land (Section 6.1) (see Fig. 1(a)), and then cumulus convection (Section 6.2) (Fig. 1(b)) and its self-organized structures (due to the second-kind instability) as tropical cyclones (Section 6.3) and intraseasonal variations (ISVs) (Section 6.4).

The governing equations in this chapter are almost common to those for the equatorial waves. (5.1)–(5.5), but now they are not always restricted by the hydrostatic, linear and dry approximations:

$$\frac{\overline{D}u'}{Dt} + u' \frac{\partial u'}{\partial x} + v' \left(\frac{\partial \overline{u}}{\partial y} + \frac{\partial u'}{\partial y} - f \right) + w' \left(\frac{\partial \overline{u}}{\partial z} + \frac{\partial u'}{\partial z} \right) + \frac{\partial \phi'}{\partial x} = K' \nabla^2 u', \quad (6.1)$$

$$\frac{\overline{D}v'}{Dt} + u' \left(\frac{\partial v'}{\partial x} + f \right) + v' \frac{\partial v'}{\partial y} + w' \frac{\partial v'}{\partial z} + \frac{\partial \phi'}{\partial y} = K' \nabla^2 v', \quad (6.2)$$

$$\frac{\overline{D}w'}{Dt} + u' \frac{\partial w'}{\partial x} + v' \frac{\partial w'}{\partial y} + w' \frac{\partial w'}{\partial z} + \frac{\partial \phi'}{\partial z} = \frac{R}{H} T' + K' \nabla^2 w', \quad (6.3)$$

$$\frac{\overline{D}T'}{Dt} + u' \frac{\partial T'}{\partial x} + v' \frac{\partial T'}{\partial y} + w' \left(\Gamma + \frac{d\overline{T}}{dz} + \frac{\partial T'}{\partial z} \right) = K \nabla^2 T' + \frac{L}{C_p} s, \quad (6.4)$$

$$\frac{\partial u'}{\partial x} + \frac{\partial v'}{\partial y} + \frac{1}{\rho_0} \frac{\partial \rho_0 w'}{\partial z} = 0, \quad (6.5)$$

$$\frac{\overline{D}r}{Dt} + u' \frac{\partial r}{\partial x} + v' \frac{\partial r}{\partial y} + w' \frac{\partial r}{\partial z} = K'' \nabla^2 r - s. \quad (6.6)$$

In this chapter we often neglect the variation of ρ_0 in the continuity equation (6.5) such as

$$\frac{\partial u'}{\partial x} + \frac{\partial v'}{\partial y} + \frac{\partial w'}{\partial z} = 0, \quad (6.7)$$

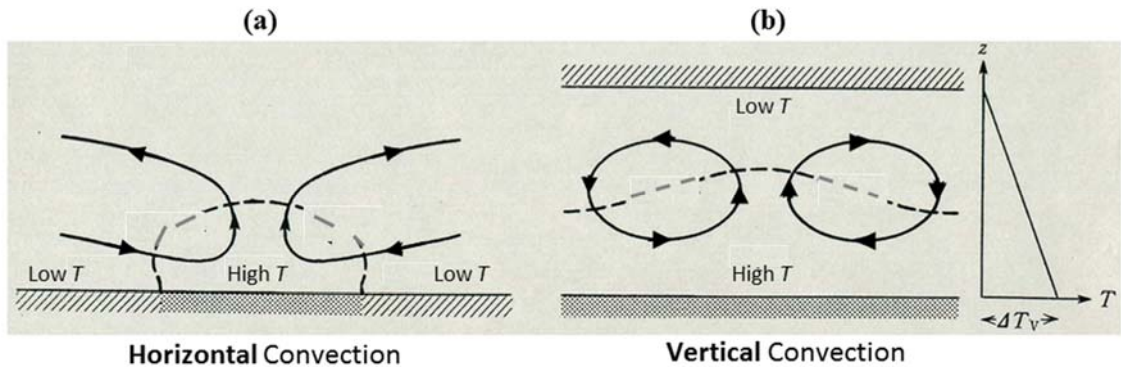


Fig. 6.1 Schematic comparison between (a) forced horizontal and (b) unstable vertical convections (modified from Ogura, 1997).

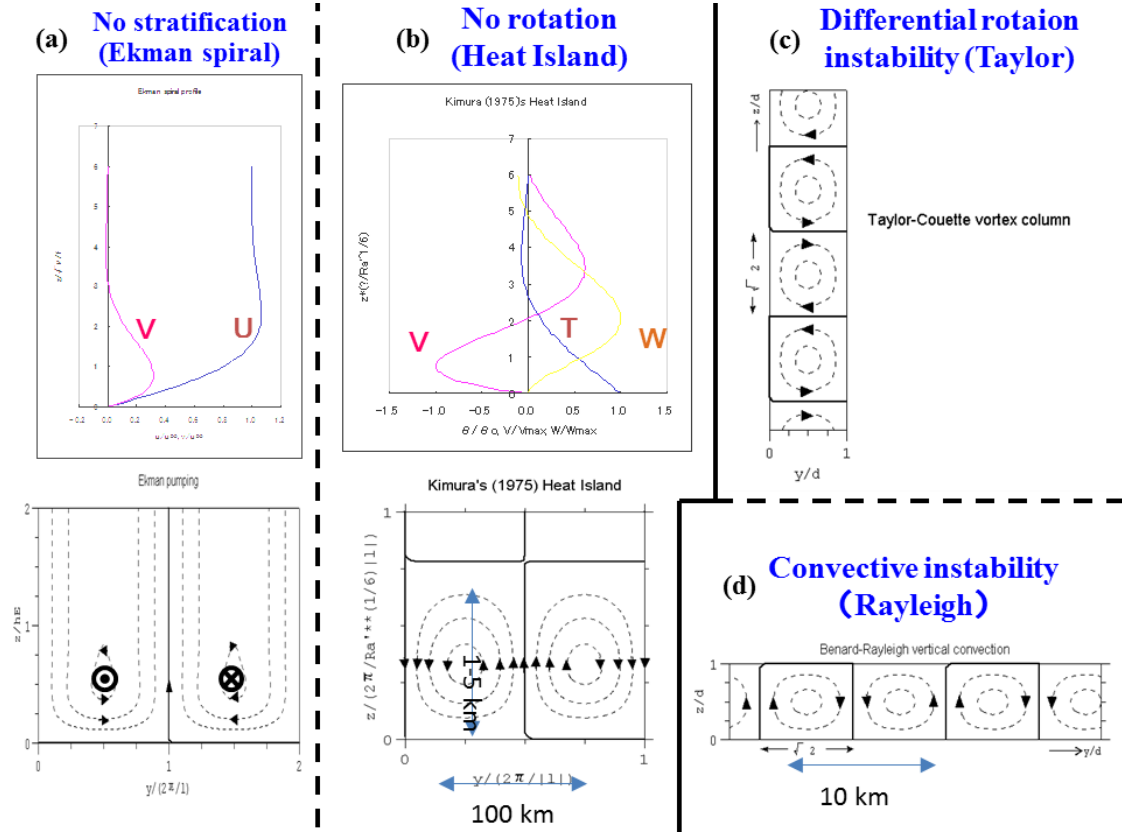


Fig. 6.2 Major solutions of the governing equation (6.9) for convection: (a) the Ekman spiral for no stratification; (b) heat-island (perpetual sea or land breeze) for no rotation; (c) Taylor’s differential rotation instability; and (d) Rayleigh’s convective instability.

in spite of keeping the buoyancy term in the vertical momentum equation (6.3), which is called the *Boussinesq approximation*. Under this approximation and the mean field varying only vertically, $\partial(6.1)/\partial z - \partial(6.3)/\partial x$ gives an equation for the meridional vorticity:

$$\eta' \equiv \frac{\partial u'}{\partial z} - \frac{\partial w'}{\partial x}, \quad (6.8)$$

as

$$\begin{aligned} \frac{\overline{D}\eta'}{Dt} + u' \frac{\partial \eta'}{\partial x} + v' \frac{\partial \eta'}{\partial y} + w' \left(\frac{d^2 \bar{u}}{dz^2} + \frac{\partial \eta'}{\partial z} \right) \\ = -\frac{R}{H} \frac{\partial T'}{\partial x} + \frac{\partial v'}{\partial y} \left(\frac{d\bar{u}}{dz} + \eta' \right) - \left[\frac{\partial v'}{\partial z} \left(\frac{\partial u'}{\partial y} - f \right) - \frac{\partial v'}{\partial x} \frac{\partial w'}{\partial y} \right] + K' \nabla^2 \eta', \end{aligned} \quad (6.9)$$

The left-hand side is the temporal variation of rotation (clockwise toward the rotation axis (y direction), as observed from the $-y$ direction) of air parcel in the xz -plane, and the right-hand side is its cause: the first term is the buoyancy torque due to a temperature gradient in the x direction (perpendicular to the rotation axis), the second term is the angular momentum conservation (rotation radius decrease) with convergence in the xz -plane (due to the velocity gradient along the rotation axis), the third term is ‘tilting’ (rotation axis direction change) of the rotations around the other (z and x) directions (these two terms do not appear if the rotation is two dimensional, that is homogeneous along the rotation axis), and the last term is the viscous dissipation. Major solutions of (6.9) are shown in Fig. 6.2.

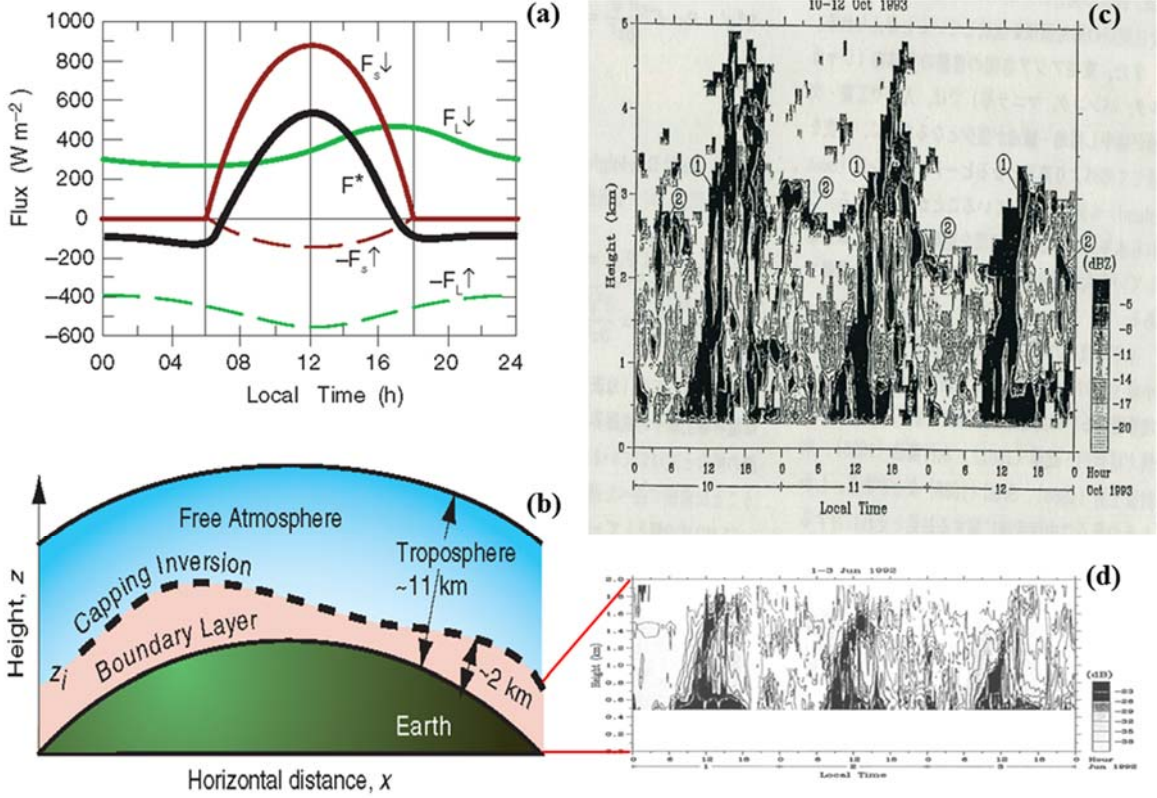


Fig. 6.3 Schematic view of (a) radiation budget (net flux (*) given by the sum of up- (↑) / down- (↓) ward fluxes of short- (S; from Sun) and long- (L; from ground) wavelengths) and (b) structure of the atmospheric boundary layer (Stull, 2006, not restricted for the tropics), and wind profiler echo (turbulence intensity and/or stratification stability) observation for three days in (c) the tropics (near Jakarta, Indonesia; Hashiguchi et al., 1995a) and (d) the extratropics (near Kyoto, Japan; Hashiguchi et al., 1995c).

Temporal variation of the integration of motion along a closed circuit in the plane of (in particular, as in Section 6.1, forced horizontal) convection becomes the integration of $\overline{D\eta'}/Dt$ over the area surrounded by the circuit (e.g., an example in Section 4.1 of Holton, 1992). This is called the *circulation theorem*, corresponding to the integration form of the vorticity equation (6.9).

6.1. Sea-land breeze circulation (Horizontal convection)

(i) Heat island (Steady local circulation):

At first let us consider a simple *horizontal convection* (Fig. 6.1(a)) forced by to a temperature gradient at the bottom under a stable stratification as parameterized by a real value of the Väisälä-Brunt frequency (4.19). For simplicity we assume two-dimensional ($v' \equiv 0$, $\partial/\partial y = 0$), no mean wind ($\bar{u}=0$), no moisture ($r \equiv 0$) and the Boussinesq approximation (6.7), we define a streamfunction ψ' such that

$$u' \equiv \frac{\partial \psi'}{\partial z}, \quad w' \equiv -\frac{\partial \psi'}{\partial x}; \quad \eta' = \frac{\partial^2 \psi'}{\partial x^2} + \frac{\partial^2 \psi'}{\partial z^2} = \nabla^2 \psi', \quad (6.10)$$

then the vorticity and thermodynamic equations (6.9) and (6.4) become

$$\left(\frac{\partial}{\partial t} - K' \nabla^2 \right) \nabla^2 \psi' = \frac{\partial(\psi', \nabla^2 \psi')}{\partial(x, z)} - \frac{R}{H} \frac{\partial T'}{\partial x}, \quad (6.11)$$

$$\left(\frac{\partial}{\partial t} - K \nabla^2 \right) T' = \frac{\partial(\psi', T')}{\partial(x, z)} + \frac{H}{R} N^2 \frac{\partial \psi'}{\partial x}. \quad (6.12)$$

These two equations are mathematically closed for two dependent variables ψ' and T' . For a horizontal convection considered here, on one hand, the horizontal temperature gradient of the second term in the right-hand side of (6.11) is always given by a bottom boundary condition (shown later in (6.14)). Thus, even if the temperature gradient is very weak, a very weak convection is generated, and if no gradient given, no convection generated. On the other hand, for a vertical (unstable or Bénard-Rayleigh) convection mentioned in the next subsection, the horizontal temperature gradient is generated automatically as a result of occurrence of convection, but the given (unstable) vertical temperature gradient HN^2/R (< 0 , N : imaginary) should be large enough to exceed the viscosity (and heat conduction).

Some of the horizontal convection follow almost completely the temporal and spatial scales of forcing, and the others are spatially restricted within a boundary layer/region (narrower than the whole scales of forcing), temporally delayed and filtered in wavenumbers and frequencies. The former examples are found around a ‘megacity’ such as Jakarta, Bangkok and Manila (called ‘heat island’) due to paved ground, many tall concrete buildings, car exhaust, air conditioners, industries, etc. making there warmer than its surrounding suburb-country area, which is considered mainly in this subsection. For the latter category is found along a coastline between broad sea and land surfaces (as considered in the next subsection). The meridional circulations and monsoons (Sections 4.3–5) with the forcing-circulation balance (4.20) are similar to the first category rather than the second category.

For a steady ($\partial/\partial t = 0$) and sufficiently weak (negligible nonlinear terms) situation of the heat island, (6.11) and (6.12) may be immediately reduced to an equation only for one variable. Assuming furthermore that the viscosity and diffusion are dominant in the vertical direction ($\nabla^2 \approx \partial^2/\partial z^2$), the equation for T' becomes

$$\frac{\partial^6 T'}{\partial z^6} + Ra' \cdot k^4 \frac{\partial^2 T'}{\partial x^2} = 0, \quad Ra' \equiv \frac{N^2/k^4}{K'K}, \quad (6.13)$$

where k is taken from (the wavenumber of spatially cyclic heating in) an appropriate boundary condition:

$$T' = \Delta T \cos kx, \quad u' = w' = 0 \left(\frac{\partial^2 T'}{\partial z^2} = \frac{\partial^3 T'}{\partial z^3} = 0 \right) \quad \text{at } z = 0; \quad (6.14)$$

$$T', u', v' \rightarrow 0 \left(\frac{\partial^2 T'}{\partial z^2}, \frac{\partial^3 T'}{\partial z^3} \rightarrow 0 \right) \quad \text{at } z \rightarrow \infty. \quad (6.15)$$

Substituting

$$T'(x, z) = \tilde{T}(z) \cdot \cos kx, \quad (6.16)$$

(6.13) is reduced to an ordinary differential equations only for z , and its solution may be obtained as

$$\tilde{T}(z) = \frac{1}{2} e^{-Ra'^{1/6} kz} + \frac{1}{\sqrt{3}} e^{-\frac{1}{2} Ra'^{1/6} kz} \cdot \cos \left(\frac{\sqrt{3}}{2} Ra'^{1/6} kz - \frac{\pi}{6} \right) \quad (6.17)$$

(Kimura, 1975). The solutions for T' , u' and v' obtained by (6.17), (6.16) and (6.10) are plotted in Fig. 6.2(b). The vertical scale of the local circulation becomes $Ra'^{-1/6}$ times of the horizontal scale. For a typical value $k \sim 2\pi/60 \text{ km} \sim 10^{-4} \text{ m}^{-1}$, $N \sim 2\pi/10 \text{ min} \sim 10^{-2} \text{ s}^{-1}$ (corresponding to $d\bar{\theta}/dz \sim 3 \text{ K/km}$) and $K \sim K' \sim 10 \text{ m}^2/\text{s}$, we obtain $Ra' \sim 10^{10}$, which implies that the ratio of horizontal/vertical scales ~ 50 times. Because the height of boundary layer on land in the tropics seems to be higher than the extratropics (2–5 km) (Hashiguchi et al., 1995a,b,c), the horizontal scale of the local circulation is expected to be 100–300 km.

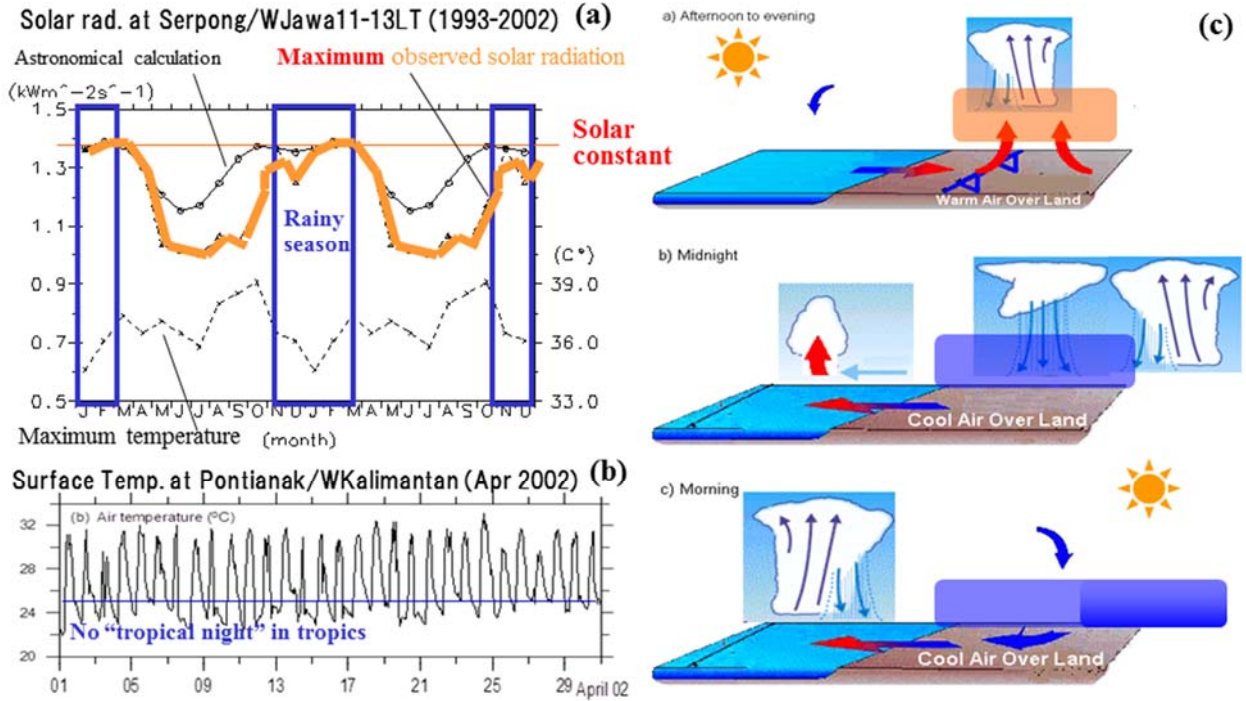


Fig. 6.4 Diurnal cycle mechanism. (a) Repeated two cycles of monthly maximum insolation (in a clear condition just before noon) at Serpong, West Jawa in 1993–2002, showing the annual maximum identified with the rainy season (Araki et al., 2007). (b) Hourly temperature at Pontianak, West Kalimantan in April 2002, showing every daily minimum lower than 25°C (Wu et al., 2008a). (c) Schematic model for the ‘sprinkler-like’ cooling the ground and surface atmosphere during midnight and morning (Wu et al., 2009b).

(ii) Sea-land (and Mountain-valley) breeze circulation:

As have been mentioned on the annual-cycle monsoons (Section 4.4), there are sea-land differences across the coastlines of oceans (and large lakes like Victoria in central Africa) on the surface insolation heating and infrared cooling, of which the (tropically much stronger) diurnal-cycle atmospheric response is the *sea-land breeze circulation*. Probably the first detailed study on this circulation in the tropics was done at Batavia (Jakarta) by van Bemmelen (1922). The solar heating in J or \bar{Q} is through complex processes of the parasol effect, land/ocean surface and atmospheric boundary-layers (e.g., Hartmann, 1994; Stull, 1988), but its variability is mainly dependent on its value calculated by the astronomical formula (cf. Fig. 6.4(a)–(b)):

$$I_s = \begin{cases} I_{s0} \left(\frac{\bar{d}}{d}\right)^2 (\sin \varphi \sin \delta + \cos \varphi \cos \delta \cos h) & \text{for daytime } (-h_0 \leq h \leq h_0) \\ 0 & \text{for nighttime} \end{cases} \quad (6.18)$$

where the solar declination angle δ and the Sun-Earth distance squared $(\bar{d}/d)^2$ concern the seasonal cycle through a diurnal integration of (6.18), as have been shown in Section 4.1.⁵⁷ In the daytime the cross-coastal temperature and pressure gradients (hotter and lower on land) induce a *sea breeze*, and its convergence with moisture transport generate strong convective clouds at a distance of the order of 100 km inland in the tropics⁵⁸. The sea breeze lower than 2–5 km on land in the tropics (Hashiguchi et al., 1995a, b, c; thicker than the extratropics and the marine

⁵⁷By this forcing the tides with global phase structures are also generated, just similar to the ‘astronomical monsoon’ in case of annual-cycle forcing.

⁵⁸Development of a distinct boundary (called the sea breeze front in the extratropics) between cooler maritime air and the continental warmer air and its movement from the coast to inland do not always appear in the tropics. *Gust front* by an individual convective cloud is much clearer (cf. Section 6.2).

atmosphere considered in Sections 5.2 and 5.3) and the upper "return" current construct a circulation, and a strong vertical shear between them may cause a Kelvin-Helmholtz instability (Hadi et al., 2000).

At night, the land cools more rapidly than the sea and a *land breeze* develops. The nighttime cooling is mainly due to the emission of infrared radiation and thus clear sky condition is preferred in the extratropics, but is due to 'sprinkler effect' associated with strong rainfall from the convective cloud developed in the afternoon and thus dominant in the rainy season in the tropics (Wu et al, 2008a; Yamanaka, 2016) (Fig. 6.4(c)). In the morning and evening the surface wind direction is reversed between onshore and offshore, but the reversal time and feature vary depending on the mean wind (averaged for 24 hours), latitude and coastal geography. In the extratropics, as inertio-gravity wavelike characteristics (to be mentioned later), the Coriolis force induces an along-shore wind component, and rotates the wind direction clockwise/anticlockwise in the northern/southern hemisphere. Furthermore, another differential daytime insolation and nighttime cooling appear on the sloping terrain between mountain and valley (relatively strong and weak, respectively), inducing a *valley and mountain breeze circulation*. In the tropics, as will be mentioned later in the next subsection (iii), many areas have coastlines near mountains, and both sea-land and mountain-valley breezes are additive, which is a reason why the diurnal cycle is dominant there.

Theoretically we consider a local circulation forced by a periodical heating on the land ($x > 0$), and add a heating term $(R/H)\dot{Q}$ in the right-hand side of the thermodynamic equation (6.4). For simplicity we assume quasi-two-dimensional ($\partial/\partial y = 0$, but $v' \neq 0$), constant mean wind ($\partial\bar{u}/\partial z=0$), no moisture ($r \equiv 0$), $K' = K$ and the Boussinesq approximation (6.7), we define a streamfunction ψ' as (6.10). Then (6.11) and (6.12) for the previous problem are replaced by

$$\left(\frac{\partial}{\partial t} + \bar{u}\frac{\partial}{\partial x} - K\nabla^2\right)\nabla^2\psi' = f\frac{\partial v'}{\partial z} - \frac{R}{H}\frac{\partial T'}{\partial x}, \quad (6.19)$$

$$\left(\frac{\partial}{\partial t} + \bar{u}\frac{\partial}{\partial x} - K\nabla^2\right)v' = -f\frac{\partial\psi'}{\partial z}, \quad (6.20)$$

$$\left(\frac{\partial}{\partial t} + \bar{u}\frac{\partial}{\partial x} - K\nabla^2\right)T' = \frac{H}{R}N^2\frac{\partial\psi'}{\partial x} + \frac{H}{R}\dot{Q}. \quad (6.21)$$

Note that, if the flow v' along the coastline satisfies a thermal wind balance (4.11) with the temperature gradient $\partial T'/\partial x$ across the coastline, (6.19) may give a trivial solution $\psi' \equiv 0$ with no circulation.

Substituting $\frac{\partial}{\partial z}(6.20)$ and $\frac{\partial}{\partial x}(6.21)$ into $\left(\frac{\partial}{\partial t} + \bar{u}\frac{\partial}{\partial x} - K\nabla^2\right)(6.19)$, we have a single equation for ψ' :

$$\left[\left(\frac{\partial}{\partial t} + \bar{u}\frac{\partial}{\partial x} - K\nabla^2\right)^2\nabla^2 + N^2\frac{\partial^2}{\partial x^2} + f^2\frac{\partial^2}{\partial z^2}\right]\psi' = -\frac{\partial\dot{Q}}{\partial x}. \quad (6.22)$$

Here the spatial scale is smaller than the case considered in (5.8), and all the factors may be regarded as constants. Thus we substitute

$$(\psi', \dot{Q}) = (\tilde{\psi}, \tilde{Q})e^{i(kx+mz-\omega t)}, \quad (6.23)$$

into (6.22), and obtain, using (5.9),

$$\{[(\hat{\omega} + iK(k^2 + m^2))^2 - N^2]k^2 + [(\hat{\omega} + iK(k^2 + m^2))^2 - f^2]m^2\}\tilde{\psi} = -ik\tilde{Q}. \quad (6.24)$$

If K is sufficiently large and N , $|f|$ and $|\tilde{Q}|$ are all not so large, then we may assume an imaginary part ω_i of ω , and (6.24) gives

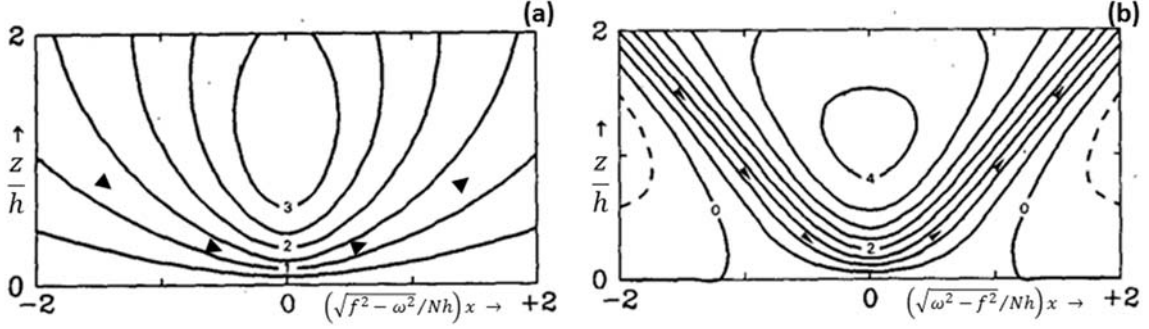


Fig. 6.5 Streamlines $\psi'/(h^2\omega)$ (h : a vertical scale; $\omega \equiv 2\pi/1\text{day}$) as solutions of (6.22) in the vertical plane perpendicular to the coastline ($x > 0, z = 0$: land surface; $x < 0, z = 0$: sea surface) under no mean flow ($\bar{u} = 0, \hat{\omega} = \omega$) for (a) the extratropics ($|\varphi| > 30^\circ, |f| > |\hat{\omega}|$) at 'noon' ($\omega t = \pi/2$) and (b) the tropics ($|\varphi| < 30^\circ, |f| < |\hat{\omega}|$) at 'sunset' ($\omega t = \pi$) (Rotunno, 1983).

$$\omega_i = -K(k^2 + m^2), \quad \text{i.e., } \psi' \propto e^{-i\omega t} \propto e^{\omega_i t} = e^{-K(k^2 + m^2)t},$$

which corresponds to a damping motion due to viscosity/diffusion. If K and $|f|$ are both large, and the situation is steady and horizontally uniform ($\omega = 0, k = 0$), then we assume a complex vertical wavenumber $m \equiv m_r + im_i$, and (6.24) becomes

$$K^2 m^4 + f^2 \approx 0, \quad \text{i.e., } m_r^2 \approx m_i^2 \quad \text{and} \quad 2m_r m_i \approx \frac{f}{K}, \quad \text{i.e., } m \approx (-1 + i) \sqrt{\frac{|f|}{2K}}$$

(other roots are inappropriate), which gives (under boundary conditions: $(u', v') = 0$ at $z = 0$ and $(u', v') \rightarrow (u_\infty, 0)$ as $z \rightarrow \infty$) so-called *Ekman's spiral hodograph*:

$$(u' - u_\infty, v') \approx u_\infty e^{-\frac{z}{\delta_E}} \left(-\cos \frac{z}{\delta_E}, \sin \frac{z}{\delta_E} \right), \quad \delta_E \equiv -\frac{1}{m_r} = \frac{1}{m_i} = \sqrt{\frac{2K}{|f|}}. \quad (6.25)$$

This result does not include any thermal conditions such as the heating \tilde{Q} (although N -dependency might be included in K), but δ_E is a good approximation for the boundary layer top in the extratropics ($\delta_E \sim 1.4$ km for $K \sim 10^2$ m²/s and $|f| \sim 10^{-4}$ s⁻¹). However, it can hardly be applied in the tropics, where $|f|$ is small and \tilde{Q} is essentially important due to large moisture and strong heating.

When K is small, (6.24) becomes

$$[(\hat{\omega}^2 - N^2)k^2 + (\hat{\omega}^2 - f^2)m^2]\tilde{\psi} = -ik\tilde{Q}. \quad (6.26)$$

If the heating \tilde{Q} is omitted, the (free) solution must satisfy the inside of the left-hand side bracket being zero, which is just the dispersion relation for the inertio-gravity waves (5.16) (for $l = 0$ and $|\hat{\omega}|$ not neglected for N). This is why the wind direction rotates clockwise/anticlockwise in the northern/southern hemisphere. As mentioned for the Hadley circulation (Section 4.3), the horizontal convection may be given by a superimposition of upward and downward propagating internal waves, which in total satisfy the bottom boundary condition of zero vertical velocity (Fig. 2.7). Thus, as mentioned in Section 5.1, any disturbances (including those forced by \tilde{Q}) satisfying $|f| < |\hat{\omega}| < N$, may be propagating vertically, and the other modes must be decaying vertically (upward, if the heating sources are at the bottom) (Rotunno, 1983) (Fig. 6.5). For the sea-land breeze circulation the heating \tilde{Q} is originated from the insolation (6.18) with the diurnal cycle, of which the frequency $\omega = 2\pi/1$ solar day = $2\pi/24$ h = 7.272×10^{-5} s⁻¹. Because the Coriolis parameter (without using the β -plane approximation (4.7)) is given by $f = 2\Omega \sin \varphi$, where

$\Omega = 2\pi/1$ sidereal day $= 2\pi/(24 \text{ h} \times 365/366) = 7.292 \times 10^{-5} \text{ s}^{-1}$, the diurnal cycle frequency should satisfy $|\hat{\omega}| > |f|$ approximately for $|\varphi| < 30^\circ$, if \bar{u} is sufficiently weak. Therefore, it is expected that the sea-land breeze circulation must be dominant in the tropics.

It is known, in addition to the shear layer between the surface sea wind and the return flow mentioned before, that a *sea-breeze front* exists as the rather clear-cut leading edge of the sea-wind region, at which convective clouds associated with showers, thunders and gusts are often organized (although a smaller-scale gust front with individual cloud is also remarkable). In the coasts near steep mountains a land- (or mountain-) breeze front with similar features is also observed, which appears typically during torrential rainfalls in the IMC (e.g., Wu et al., 2007). The horizontal scale λ_d of the sea-land breeze circulation cells and the migrations of such frontal structures may be given essentially by the dispersion relation of internal gravity waves (e.g., Rotunno, 1983; Niino, 1987): from (6.26) or (5.16)

$$\lambda_d \approx \frac{2\pi}{|k|} = \sqrt{\frac{N^2 - \hat{\omega}^2}{\hat{\omega}^2 - f^2}} \frac{2\pi}{|m|} \approx \frac{N}{|\hat{\omega}|} h_d \approx \frac{\sqrt{gh}}{\tau}, \quad (6.27)$$

where h_d is the height of the sea-land breeze circulation cell and $\tau = 2\pi/1$ day. Observationally $\sqrt{gh} \sim 5\text{--}10$ km/h $\approx 1\text{--}3$ m/s (one order slower than that for the large-scale equatorial waves), $h_d \sim 2\text{--}5$ km, and $\lambda_d \sim 100\text{--}300$ km (see the next subsection (iii)).

More realistic intermediate cases include the both aspects mentioned above (e.g., Niino, 1987). If the forcing is not vertically wavy like (6.23) but limited at the bottom like the steady heat island case mentioned in the previous subsection (i), the vertical extension is controlled also with viscosity/diffusivity as $\propto Ra'^{-1/6} \propto K^{1/3}$ in (6.13) or as $\delta_E \propto K^{1/2}$ in (6.25). ‘Roll’ structures (associated with banded clouds actually) due to convective and shear instabilities generated locally at around the sea-breeze front are also studied theoretically (Asai, 1970, 1972; partly mentioned in the end of Section 6.2(i)). Realistic nonlinear numerical studies on the sea-land breeze circulations were pioneered by Filipino meteorologist Estoque (1962), who considered Manila Bay at about 15°N with Coriolis force and background wind. Sun and Orlanski (1981a, b) showed both linear analytical and nonlinear numerical solutions for the sea-land breeze circulations which are gravity-wavelike and dependent on the Coriolis force. Some studies without the Coriolis force (e.g., Fovell, 2005) may be applicable also for the equatorial tropics, which will be mentioned briefly again the next section. Recent high-resolution models simulating the equatorial sea-land breeze circulations show various differences from the extratropics (Saito et al., 2001; Wu et al., 2003; Sasaki et al., 2004; Arakawa and Kitoh, 2005; Hara et al., 2009; Sato et al., 2009) (see Figs 6.4(c), 6.6–6.9). More details and other aspects of the diurnal-cycle sea-land (and mountain-valley) breeze circulations are mentioned in several mesoscale and boundary-layer meteorology textbooks (e.g., Stull, 1988; Lin, 2007), although most descriptions are on the extra- or sub-tropics.

Because the sea-land circulation is a superimposition of upward and downward propagating internal gravity waves, the former may be regarded as a source of the latter, in particular those propagating until the middle and upper atmospheres (cf. Section 5.4). Their propagations are modified if the background wind is changed. Actually the amplitude distributions of gravity waves in the lower stratosphere (Fig. 5.4(h)–(i)) resemble those of convective activity and their cause (solar radiation) (Fig. 4.6(a)). Local instability and turbulence generation has been also observed at the cloud top (e.g., Mega et al., 2010, 2012). The spectral features of cloud top temperature

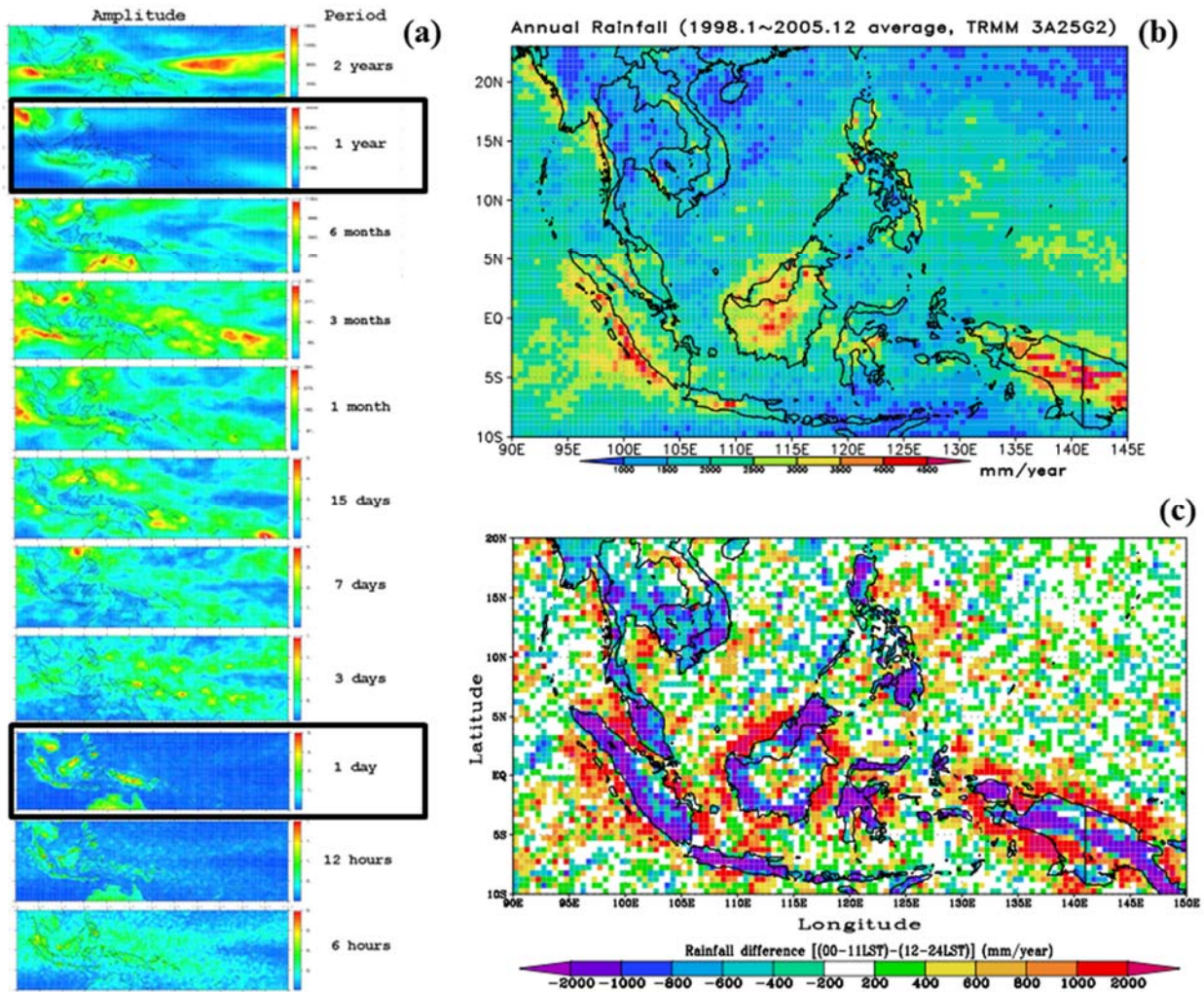


Fig. 6.6 Geographical distributions of (a) power spectral densities of 6 h–2 year components of cloud top temperature variations analyzed from 14-year hourly Geostationary Meteorological Satellites (GMS) – infrared (IR) data (Yamanaka, 2016), and (b) annual amount and (c) AM-PM difference of 3-year TRMM-PR rainfall data over the Indonesian maritime continent (Mori et al., 2004)

(corresponding to height of cloud convection) are also similar to so-called universal shapes of gravity waves (e.g., Gage and Nastrom, 1985; Nastrom and Gage, 1985; Hashiguchi et al., 1997). Generations of gravity waves from cloud systems actually observed over the IMC and their emissions to the whole middle atmosphere have been simulated by numerical models (e.g., Horinouchi and Yoden, 1996; Horinouchi et al., 2002, 2003). Momentum flux of such gravity waves have been requested to simulate the stratospheric dynamics such as equatorial quasi-biennial oscillations (Sato et al., 1999; Kawatani et al., 2010a, b), which implies also a link between climates in the troposphere and stratosphere (e.g., Kawatani and Hamilton, 2013). Furthermore the global-vertical structures of diurnal tides are also studied, in particular on their excitation/amplification in the tropics (e.g., Sakazaki et al., 2012, 2015).

(iii) Diurnal cycle dominancy in the IMC and other regions

Because the IMC is not a continent but an archipelago, it has very long coastlines surrounding large/small islands, where the diurnal-cycle sea-land breeze circulations with convective activity are generated (see, e.g., Johnson, 2011; Yamanaka, 2016). The atmosphere has high humidity (which is conditionally unstable as mentioned in the next subsection), and convective clouds are generated on land in the afternoon until evening, as shown in Fig. 6.6 (Houze

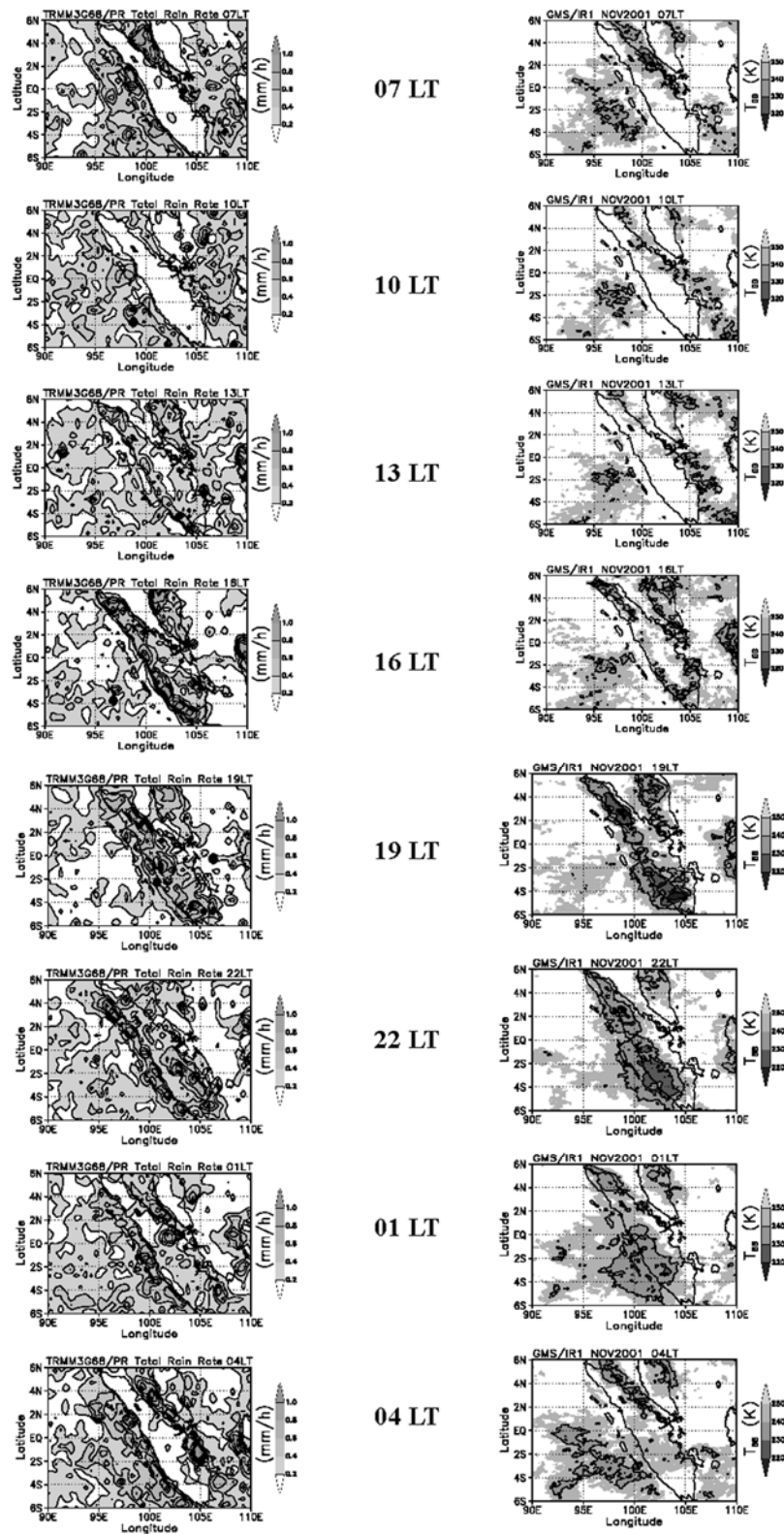


Fig. 6.7 Diurnal cycles of TRMM (on a Sun-nonsynchronous low-Earth orbit) rainfall averaged for 1998-2000 and GMS cloud top temperature averaged for November 2001. Modified from Mori et al. (2004). For GMS data also see Sakurai et al. (2005).

et al., 1981; Hendon and Woodberry, 1993; Nitta and Sekine, 1994; Hashiguchi et al., 1995; Sugimoto et al., 2000; Yang and Slingo, 2001; Ohsawa et al., 2001; Kubota and Nitta, 2001; Renggono et al., 2001; Hadi et al., 2002; Murata

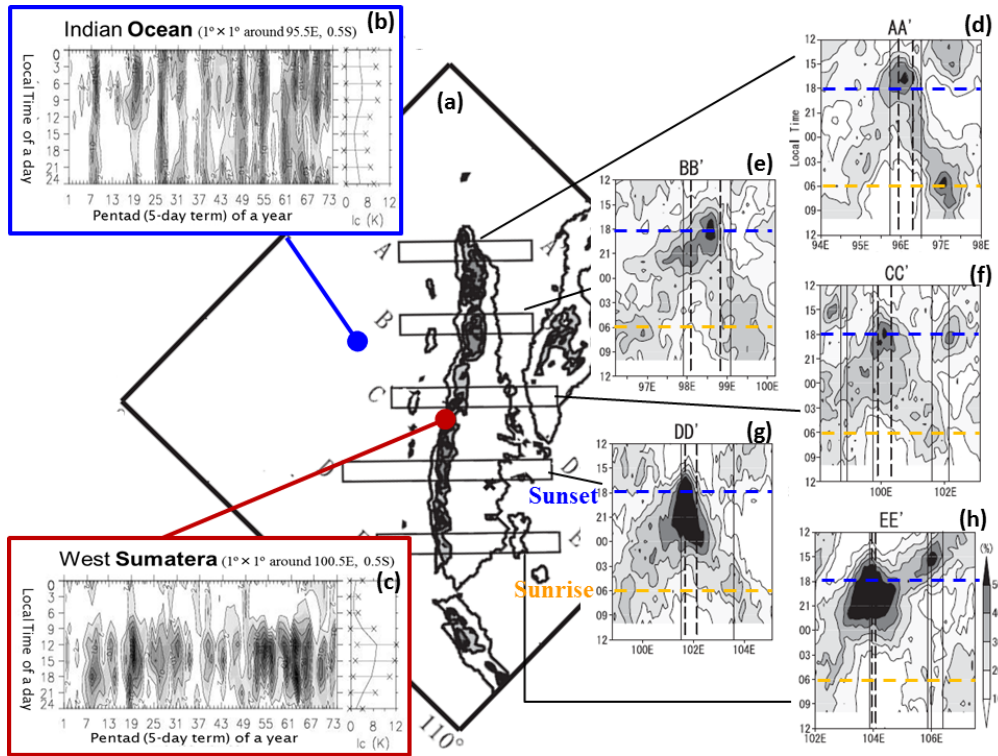


Fig. 6.8 Diurnal cycles of cloud top temperature (a) around Sumatra, shown by seasonal-local time variations on (b) the Indian-Ocean and (c) and western coast inland (Sakurai et al., 2005) and (d)-(h) five zonal-local time variations (Hamada et al., 2008).

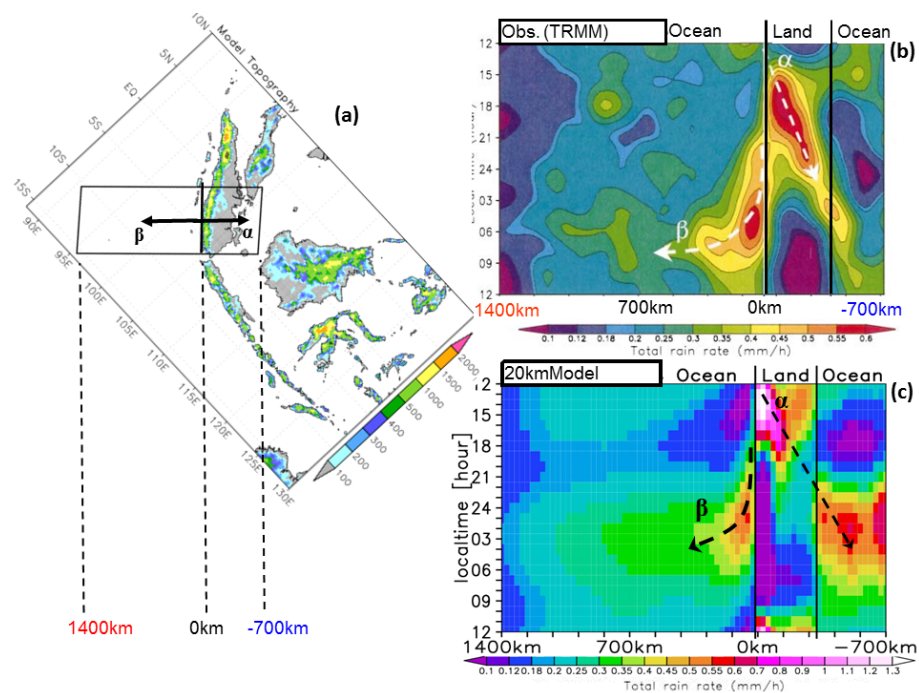


Fig. 6.9 Zonal-local time variations of diurnal-cycle rainfall migrations (a) along a section of Sumatra (b) observed by TRMM (Mori et al., 2004) and (c) analyzed from a global high-resolution numerical model (Arakawa and Kitoh, 2005).

et al., 2002; Sorooshian et al., 2002; Wu et al., 2003; Mori et al., 2004; Sakurai et al., 2005; Araki et al., 2006; Tabata et al., 2011b; and many others). The diurnal cycles over the IMC are dominant even in the rainy season (austral summer in Jawa and Bali), because rainfall-induced sprinkler-like land cooling reverses the trans-coastal temperature

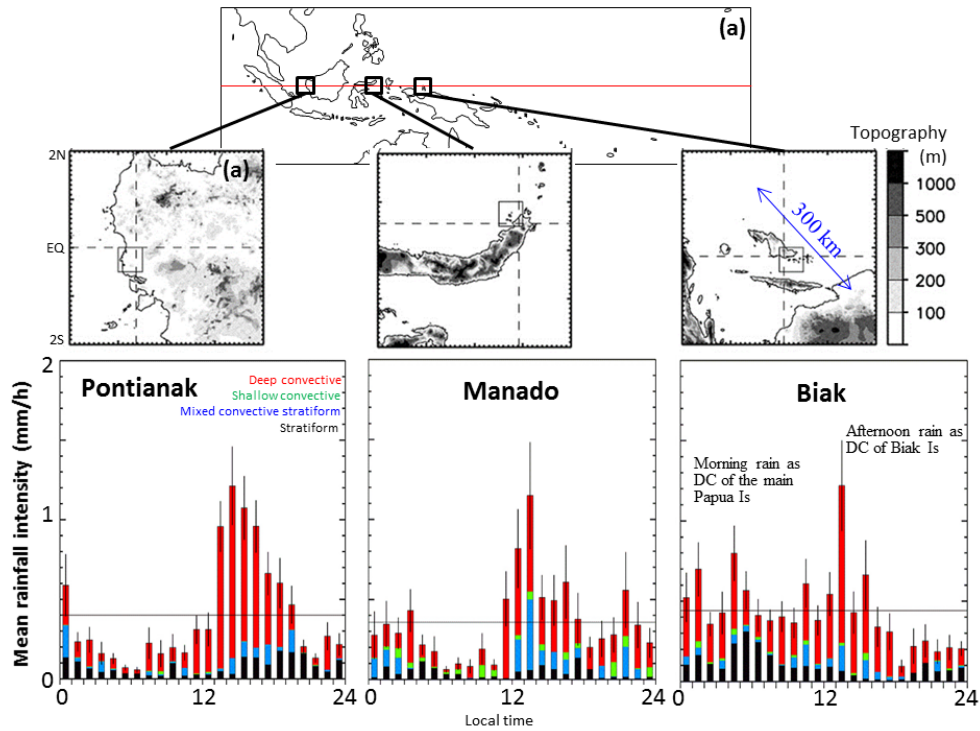


Fig. 6.10 Diurnal cycles of rainfall intensity observed by wind profilers at Pontianak (Kalimantan), Manado (Sulawesi) and Biak (near Papua) (Tabata et al., 2011b). Rainfall is classified as stratiform (black), mixed stratiform/convective (blue), shallow convective (green) and deep convective (red) types. A small island Biak has afternoon and dawn (main-island sea-side) peaks.

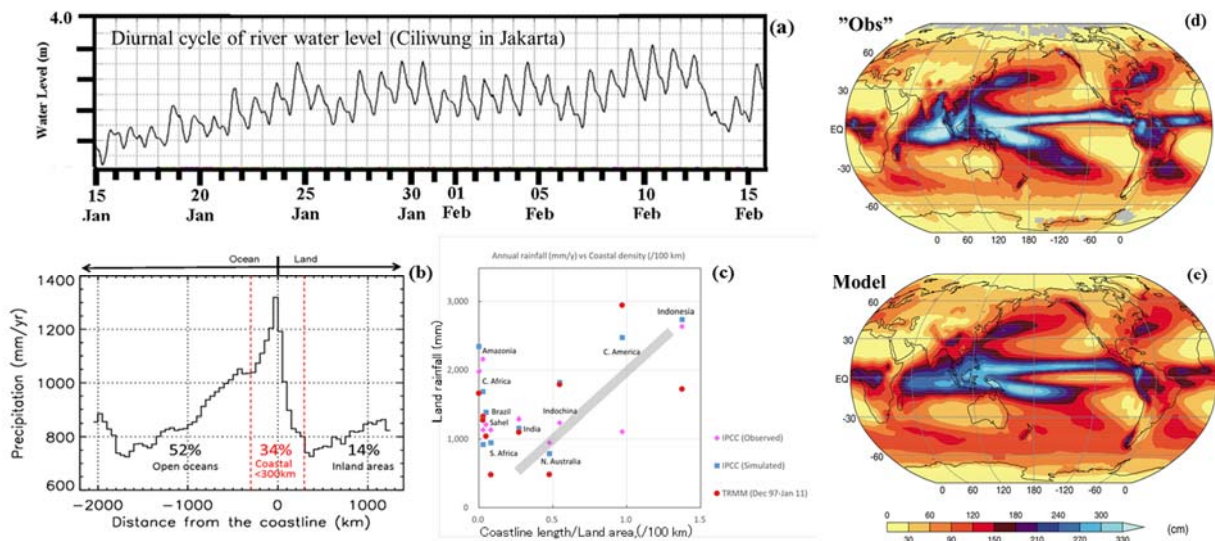


Fig. 6.11 (a) Diurnal cycle observed at a river in west Jawa (Sulistyowati et al., 2014), (b) rainfall as a function of the coastal distance over the tropics observed by TRMM (Ogino et al., 2016) and (c) regional rainfall as a function of the coastal ‘density’ (= length/area in 100 km resolution) over the tropics (modified from Yamanaka, 2016) calculated based on TRMM observations and calculated from (d) observation and (e) model of IPCC (2007).

gradient before sunrise (Fig. 6.4(c)), and subsequent clear sky on land until around noon provides solar heating dependent on season (Wu et al., 2008a).

In the western coast of Sumatera as one of the most remarkable places of the diurnal cycle (Mori et al., 2004), a convective rainfall peak appears near the coastline in the daytime and migrates toward inland until the evening (see Figs. 6.7–6.9). Another equally convective-stratiform rainfall peak starts from the coastline and migrates offshore

until the morning. Each rainfall peak migration has a distance up to 400 km and a speed around 10 m/s. The diurnal cycles are almost unique causes of surface winds stronger than 10 m/s (shown later in Figs. 6.15(a) and (d)) in the IMC almost free from cyclones (except for a rare case as shown later in Fig. 6.19). Although a local wind called “Sumatras” has been known (e.g., Scott, 1956; Nieuwolt, 1968; Chen et al., 2014), probably partially due to steep mountains (up to 3,800 m), strong winds appear near active convective clouds usually in local evening with diurnal cycle. Seasonal and meridional variations of the diurnal cycle in Sumatera associated with the ITCZ displacement have been analyzed (Sakurai et al., 2005).

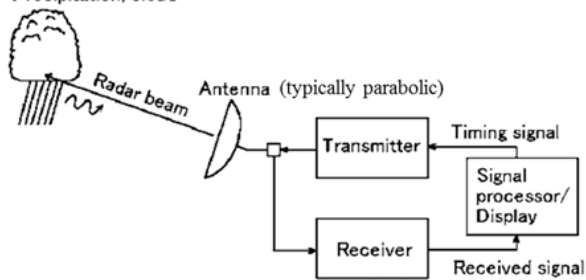
As shown in Figs. 6.8(b) and (c) very clearly, the most dominant mode is changed to the diurnal cycle near the coastline, from ISVs on the open ocean (see Section 6.4, including interactions of the two categories). Theoretically the horizontal scale of the diurnal-cycle sea-land breeze circulation in the low latitudes may be estimated by (6.27) as $\lambda_d \sim 100\text{--}300$ km. Observed values of λ_d in the IMC are 100 km or more (Wu et al., 2003, 2008a, 2009b; Mori et al., 2004; see Figs. 6.7–6.9), and the rainfall is concentrated in a distance within about 300 km (both on the land and sea sides) from the coastline (Ogino et al., 2016; see Fig. 6.11(b) later). Thus the land with clear diurnal cycle must be larger than 100 km, which has been suggested by earlier studies (e.g., Kubota and Nitta, 2001). In case of adjacent small and large islands (the former located inside the coastal area of the latter), the smaller one (such as Siberut in the west of Sumatera, and Biak in the northwest of Papua as shown in the right of Fig. 6.10) a little complex feature appears due to the diurnal cycles of the both islands (Wu et al., 2008b; Tabata et al., 2011b; Kamimera et al., 2012). In narrow straits such as Melaka (Malacca; between Sumatera and Malay) and Makassar (between Kalimantan and Sulawesi) the diurnal cycles of the both islands are interfered and sometimes seem to propagate from one island to the other (e.g., Ichikawa and Yasunari, 2007; Wu et al., 2009a; Fujita et al., 2011). They correspond to the confluence of wind known in particular in the Melaka Strait (e.g., Ramage, 1971; Fujita et al., 2010).

The diurnal cycles over the IMC are excited by solar radiation every day and developed almost spontaneously by processes mentioned above. Therefore, as well as their amplifications at maxima (two times a year) of solar heating and moisture transport by monsoon and/or ISVs, any suppression processes may induce their temporal/spatial variability. Larger-scale may concern such amplification and suppression, as considered since earlier studies around the IMC (e.g., Houze et al., 1981; Johnson and Priegnitz, 1981; Johnson and Kriete, 1982). Western coast predominance in comparison to eastern coast (in Sumatera and Kalimantan, as well as Malay, Indochina Peninsula and Indian Subcontinent) has been reported (cf. Figs. 6.6–6.7) and discussed in view of prevailing winds and/or gravity-wave propagations to enhance a circulation cell on the western side and suppress the other one on the eastern side (e.g., Murata et al., 2002; Mori et al., 2004; Xie et al., 2006; Wu et al., 2009a, b).

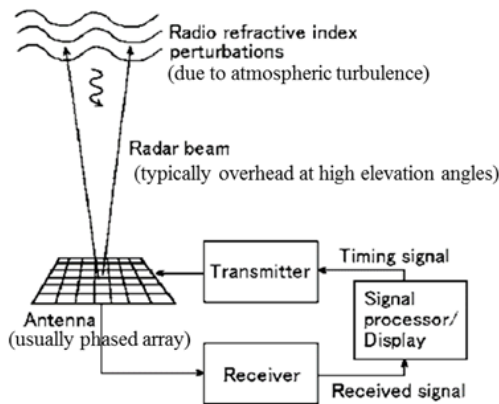
Horizontally quasi-continuous observations of rainfall over tropics with a space-borne precipitation radar on the Tropical Rainfall Measurement Mission (TRMM) launched in November 1997 have revealed that the diurnal-cycle rainfalls along the maritime-continent coastlines are heavier on the sea side (called the *coastal heavy rainband*, or CHeR) than on the land side (Mori et al., 2004, 2011; Wu et al., 2008a, 2009b). Prior to them several observational (e.g., Chang et al., 2004a) and numerical (e.g., Ogura and Yoshizaki, 1988) studies noticed substantially similar phenomena of convective activities and considered mainly orography (mountain range) effects on monsoons. After starting TRMM other studies for various areas in tropics (e.g., Xie et al., 2006) also noticed what we call CHeR, and studied mainly the orographic effect. Mechanisms generating the sea-side dominance have been shown numerically

(a) Meteorological (or weather) radar

Any hard targets/scatterers
(including aircrafts, ships, ..., birds, insects, seeds, ..., dusts, ashes, ...)
Precipitation, cloud from factories/volcanos



(b) Wind profiler (or atmospheric radar)



(c) Z (reflectivity) -R (rainfall) relationship

$$Z = AR^b$$

- I: Diffused heavy thunderstorm echo / tall evaporating echo
- II: Core of thunderstorm / intense solid echo
- III: Generating / developing intense cells
- IV: Small solid airmass echoes, scattered / lined up with rainband
- V: Stratified plane echo / weak diffused echo
- VI: completely diffused thunderstorm echo

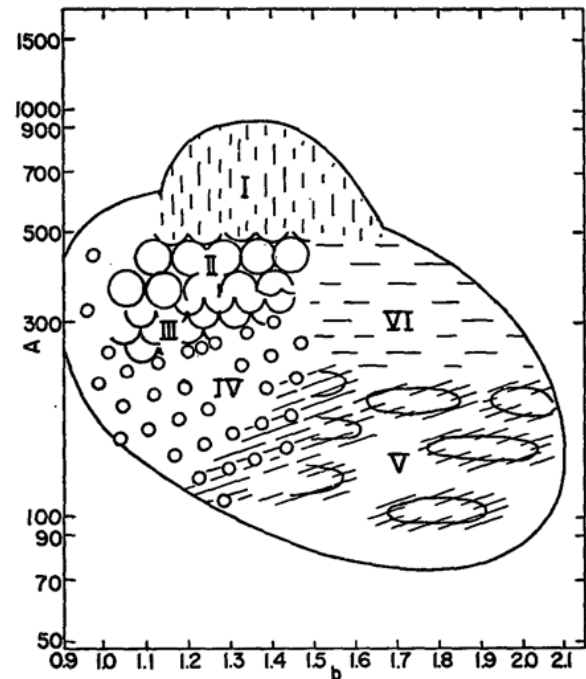


Fig. 6.12 Principles of (a) meteorological radar and (b) wind profiler (Fukao and Hamazu, 2014), and (c) the so-called Z-R relationship for meteorological radars (Fujiwara, 1965).

(Wu et al., 2008, 2009b) by nocturnal outflow (land breeze) and seaward migration of land clouds. It is shown very recently (Ogino et al., 2016) that tropical rainfall may be approximately expressed in general by a function of the coastal distance with dominance on the sea side.

The success of TRMM (including many other results which cannot be mention in this article) showed not only the scientific importance of such smaller-scale diurnal cycle, but also the technical necessity of radar remote sensing facilities (cf. Fig. 6.12) to cover the tropics for both scientific and operational objectives. Some subtropical southeast Asian countries (e.g., Malaysia, Thailand and Philippines) installed meteorological radars relatively earlier, mainly to watch typhoons. The central maritime continent – Indonesia started to install advanced operational radars since 2006, after a long history from (each few) intermittently operated old radars and research-use wind profilers (mainly on atmospheric vertical coupling; see Hashiguchi et al., 1995a; Fukao, 2006) and meteorological Doppler radars (Yamanaka et al., 2008, 2017) and now reach 40 stations covering almost the whole archipelago (Fig. 6.13).

Complex shaped coastlines such as bays and peninsulas generate convergence/divergence and other interactions of local flows. In particular in the western coasts of Sumatera Island, Indochina Peninsula (Myanmar-Thailand-Malay) and Indian Subcontinent, steep slopes of mountains (Barisan, Arakan-Tenasserim, and Western Ghāts) are located within a few hundred kilometers of the coast, sea breezes and terrain effects appear in combination. It has been known (e.g., Sorooshian et al., 2002; Mapes et al., 2003a, b; Warner et al., 2003) over the Central America that

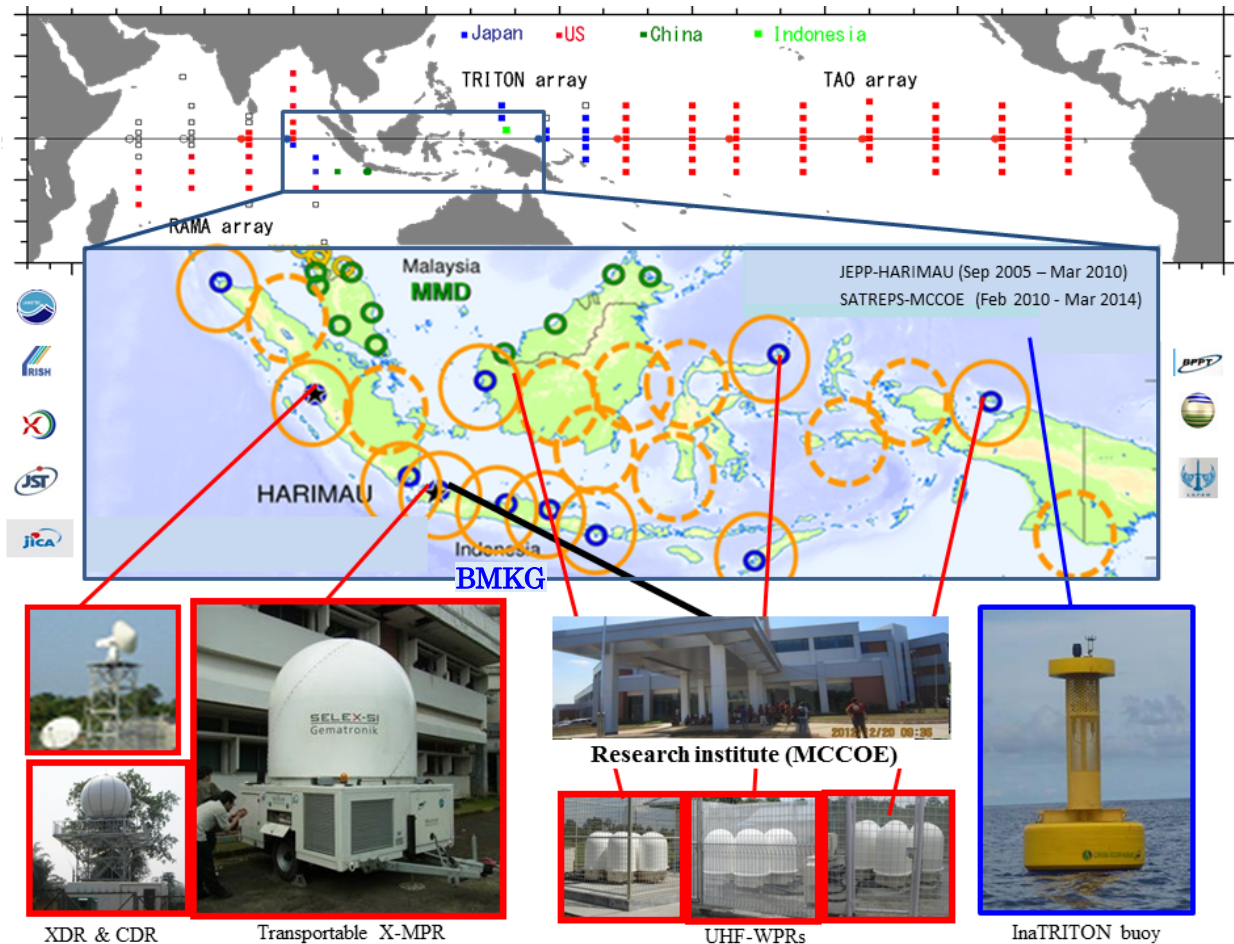


Fig. 6.13 Observation networks used in JEPP-HARIMAU (2005-2010) and SATREPS-MCCOE (2010-2014) projects (Yamanaka et al., 2008, 2017), collaborating international buoy arrays (upper map) and Indonesian operational radars (lower map; around 2010).

sea and upslope winds produce strong low-level convergence and convective rainfall over slopes of mountains (Sierra Madre de Chiapas) from afternoon to evening, and that land and katabatic winds produce convergence and convection over the offshore in particular of bay-like portions of the coastline (such as the Gulf of Panama).

The dominance of diurnal cycles suggests that the hydrologic cycle is very quick over the IMC. It has been observed and understood well (since Wu et al., 2003; Mori et al., 2004) that rainfall comparable to the annual amount (both on the sea and land sides of the coastlines) and water vapor transport by sea winds are clearly following the diurnal cycle. A recent study (Sulistyowati et al., 2014) has shown a diurnal cycle of river water level (Fig. 6.11(a)), that is, water transport from land to sea, which must be balanced with sea-wind water-vapor transport, if the water budget is closed in a river basin, a coastal sea just outside the river mouth and the atmosphere over them. This hypothesis is not so bad, because all of river flow, sea-land breeze circulation and raincloud migration are approximately perpendicular to the coastline, and also because the water is conserved by so-called cold trap mechanism at the top of tall convective clouds near the very low-temperature tropopause (often around -80°C or cooler; see e.g., Holton et al., 1995) which also follow the diurnal cycle. Although quantitative evidence has not yet been sufficient, if the evaporation from sea surface and evapotranspiration from land surface also follow the diurnal cycle, this hypothesis should hold. By this very quick water cycle, the water is almost conserved, whereas the (sensible and latent) heat transport from the earth's surface to the whole troposphere is effective enough to satisfy the

global energy budget.

Concerning interannual variations of rainfall correlated strongly (at least partly) with ENSO/IOD (Section 5.3), we may consider amplitude modulations of the diurnal cycle associated with variations of SST. Because the sea-land breeze circulations are directly enforced by the land-sea temperature difference (e.g., Estoque, 1962; Rotunno, 1983; Niino, 1987), cooler SST in El Niño and/or positive dipole mode may induce weaker land breeze and suppress sea-side rainfall in the early morning than in La Niña and/or negative dipole mode. Complex topography of coastlines, land surfaces and ocean bottoms may induce highly inhomogeneous regionality of correlations between atmosphere and ocean interacting each other. Relationship with ISVs and the diurnal cycle may be also similar (cf. Section 6.4). Serious flood events were caused by the diurnal cycles amplified by La Niña/negative IOD, transequatorial boreal winter monsoons (cold surges from Siberia) and ISVs (Wu et al., 2007, 2013), although the general relationship among the diurnal cycle, ISV, monsoon and ENSO/IOD is still a target for future studies.

It is the diurnal-cycle rainfalls along the world's longest coastlines associated with many large islands of the IMC that generate the equatorial rainfall peak controlling the global climate (see Fig. 6.11(c)). The rainfall concentration is about 2,000 mm/year for a “coastline density” 10^{-2} km^{-1} (corresponding to 102 km coastline around 10^4 km^2 area), which is consistent with the coastal peak 1,300 mm/year in Fig. 6.11(b) and also with the equatorial rainfall peak 2,000 mm/year in the middle panel of Fig. 4.6, considering that the total tropical coastline length (almost in the IMC) is almost equivalent to the equatorial circumference (40,000 km). Although it has been explained often directly by the warmest seawater surrounding the IMC, rainfall over the open ocean is less than over the islands in the IMC (cf. Qian, 2008). Indeed the solid land is heated easier than the liquid sea, but convective precipitating clouds generated over the true continents (Africa and South America) are less active than over the IMC as seen in Figs. 6.11(d)–(e) obtained from IPCC (2007) for example. Instead the diurnal cycles generated around the longest coastlines of the IMC are essential to generate the largest rainfall there. For each heavy rainfall condition produced by large-scale phenomena such as ENSO/IOD (Section 5.3), monsoon surges (Section 4.4) or ISVs (Section 6.4), only some areas have actual heavy rainfalls (Wu et al., 2007, 2013), but an integration over the long coastlines may achieve the world's largest annual rainfall amount over the IMC.

The relationships (shown in Figs. 6.11(b)–(c)) indicating importance of the local diurnal cycles imply that a climate model needs to resolve the equatorial coastlines with a scale sufficiently smaller than 100 km. Actually, recent global models have satisfied such high resolutions (e.g., Neale and Slingo, 2003; Arakawa and Kitoh, 2005; Hara et al., 2009; Satoh et al., 2008; Sato et al., 2009; Love et al., 2011). Their downscaling and regional model applications are also progressed for usual diurnal cycles (Wu et al., 2003, 2008a, 2009a, b) and extreme rainfalls making floods (Trilaksono et al., 2011, 2012).

6.2. Conditional instability and clouds (Vertical convection)

(i) Convective (Rayleigh-Taylor) instability for dry atmosphere

The vertical convection is generated spontaneously by the convective instability ($N^2 < 0$). Although in the actual atmosphere it cannot be separated from the moist (cloud condensation) processes (Chapter 3), at first we shall consider purely dynamical processes of the dry convective instability. The simplest case is a linear steady problem of which the basic equation is essentially the same as (6.13) but here without neglecting the horizontal viscosity and

diffusion:

$$\nabla^6 \psi' - Ra \cdot d^{-4} \frac{\partial^2 \psi'}{\partial x^2} = 0, \quad Ra \equiv \frac{(-N^2)d^4}{K'K}, \quad N^2 < 0, \quad (6.28)$$

where Ra is non-dimensional and called the *Rayleigh number*, and d is the height of the unstable layer given in the boundary condition:

$$\frac{\partial u'}{\partial z} = w' = T' = 0 \quad \left(\psi' = \frac{\partial^2 \psi'}{\partial z^2} = \frac{\partial^4 \psi'}{\partial z^4} = 0 \right) \quad \text{at } z = 0, d. \quad (6.29)$$

Physical differences from the forced horizontal convection under stable stratification have been mentioned below (6.12) in the previous section.

Lord Rayleigh showed that a roll-type convection with an axis along the y -direction satisfying (6.29):

$$\psi' \propto \sin kx \sin \frac{n\pi}{d}z, \quad n = 1, 2, 3, \dots,$$

may be a solution of (6.28) under the following necessary condition:

$$Ra = \frac{[k^2 + (n\pi/d)^2]^3}{k^2/d^4} \geq \frac{27}{4}\pi^4 \equiv Ra_c \quad \left(\text{equality at } n = 1, \quad kd = \frac{\pi}{\sqrt{2}} \equiv k_c d \right), \quad (6.30)$$

where Ra_c is called the critical Rayleigh number, k_c is called the critical wavenumber, and n is the number of rolls in the vertical direction. Therefore the convection of vertically one cell structure ($n = 1$) should be generated $Ra \geq Ra_c \approx 660$, and the horizontal size of the roll convection is $\pi/k_c = \sqrt{2} \approx 1.4$ times of the height d , as have been shown in Fig. 6.2(d). The other vertically multi-cell convections ($n \geq 2$) must be generated much larger (much unstable) Ra , for which always the one-cell ($n = 1$) has been developed earlier, thus they do not appear actually. The condition (6.30) is mathematically equivalent to a shear instability of flow between differentially rotating cylinders studied by G. I. Taylor (replacing the buoyancy torque in Rayleigh's problem by the centrifugal torque), and often called the *Rayleigh-Taylor instability*.

For a three-dimensional problem the solution becomes tetragon cells:

$$\psi' \propto \sin kx \sin ly \sin \frac{n\pi}{d}z, \quad n = 1, 2, 3, \dots,$$

and in the condition formula (6.30) the zonal wavenumber k is replaced by the horizontal wavenumber $\sqrt{k^2 + l^2}$. These are called the *Bénard-Rayleigh convections*⁵⁹. Numerical and laboratory experiments have shown that the results are also dependent on the Prandtl number $Pr \equiv K'/K$. If Pr is $10^1 - 10^2$, two-dimensional rolls appearing for smaller Ra are took over by three-dimensional cells at beyond $Ra \sim 10^4$, and become turbulence at around $Ra \sim 10^5$. Among many studies, Lorenz (1963) studied a much simplified (truncated) problem consisting only of the amplitude (dependent only on t) of w' and horizontal and vertical variation parts of T' of a two-dimensional-roll mode of innumerable solutions of (6.11) and (6.12). He showed that, if Ra is sufficiently large, alternative oppositely-rotating rolls (which are steady if Ra is small) continue to replace each other nonperiodically. This *deterministic chaos* depicted an essential aspect of dynamics of fluid including the Earth's atmosphere, that is, a difficulty concerning meteorological forecasts and climatological predictions, and has been applied for many physical

⁵⁹In 1900 Bénard discovered hexagonal cells generated in a thin fluid layer heated at the bottom. In 1916 Rayleigh proposed the convection theory and obtained the two-dimensional rolls. By many studies following them, the cell shape (hexagon or tetragon) is dependent on experimental conditions, and the original Bénard's experiments were governed mainly by surface tension.

and mathematical fields.

The convection theories mentioned above are still a major part of general fluid dynamics, but the unstable stratification $N^2 < 0$, i.e., $\partial\bar{\theta}/\partial z < 0$, i.e., $\partial\bar{T}/\partial z < -\Gamma$ appears very rarely in the actual atmosphere even in the tropical atmosphere heated very much by the insolation. Even if the thermal stratification is stable ($N^2 > 0$), there may be shear instabilities. If a vertical shear $\partial\bar{u}/\partial z$ exists, and the Richardson number Ri defined in (4.19) satisfies $0 < Ri < 1/4$ (Miles, 1961; Howard, 1961), strong roll-type disturbances (called ‘cat’s eye’, and seen as ‘billow clouds’) are generated (the *Kelvin-Helmholtz instability*). If the shear is strong in case of unstable stratification (Ri is small negative), rolls with axis along the background flow \bar{u} are predominant (Asai, 1970), which may explain cloud patterns over the Sea of Japan, the East China Sea and the Pacific Ocean during strong winter monsoons in the extratropics. Other (symmetric or baroclinic) shear instabilities with stable stratifications ($1/4 < Ri < 1$ or $Ri > 1$; cf. Section 4.2) are essentially important for the extratropical frontal and cyclonic disturbances, but not so in the tropical troposphere.

(ii) Conditional instability for moist atmosphere

It is the moist process that destabilize the atmosphere in particular in the tropics, although its inseparable relationship with convection is somewhat paradoxical, as so far mentioned in Sections 3.3 and 6.1. Cloud condensation with strong convection (upward motion) and resulting showery rainfall in very narrow area is much more dominant than the other manner of condensation (such as making a fog in extratropical sea surface or mountain slope) by almost static cooling and slow ascending of a broad area⁶⁰. In a convection water vapor ascending with upward flow ($w' > 0$) starts condensation around an aerosol particle (*heterogeneous nuclearization*) when it reaches the lifting condensation level (Fig. 3.6). In this way liquid or solid cloud particles are formed in the gaseous atmosphere, through complex chemical and microphysical processes. Sum of them makes latent heat release in the thermodynamics for the atmosphere. In the IMC microphysical features such as raindrop size distributions and their seasonal/diurnal variations (Renggono et al., 2001, 2006; Kozi et al., 2006) and isotope ratios of rainwater indicating its origins (Ichiyanagi, 2007; Kurita et al., 2009; Fudeyasu et al., 2011; Suwarman et al., 2013) have also been observed. Importance of clouds in the tropics is far larger than in the extratropics. (cf. Fig. 4.9) since pressure field-controlling circulations generate clouds in the extratropics, whereas clouds produce circulations in the tropics. Thus the cumulus convections in the tropics are, in spite of their individual scales similar to the extratropics, not an issue of the mesoscale section but the central issue of the whole tropical meteorology.

The most basic description on the moist atmosphere has been given in Section 3.3. Substituting the saturated value r_s given by (2.7) into the specific humidity r of the equivalent potential temperature θ_e (the second equation of (3.10)) for a saturated air parcel, we have

$$\theta_e^* \equiv \theta \cdot \exp\left(\frac{Lr_s}{C_p T}\right) \text{ (saturated equivalent potential temperature),} \quad (6.31)$$

of which the conservation ($\partial\theta_e^*/\partial z = 0$) leads to the moist (pseudo-)adiabatic lapse rate Γ_m as (3.11). When the

⁶⁰This does *not* mean absence of stratiform cloud in the tropics. A matured cumulonimbus cloud is associated with an anvil extending over much broader area than the original cloud around the tropopause. Over the sea surface smog is generated in particular around the maritime continent by a forest fire in the El Nino (generally less rainfall) year. These two stratiform clouds contribute to rainfalls very little but to radiative energy budget considerably.

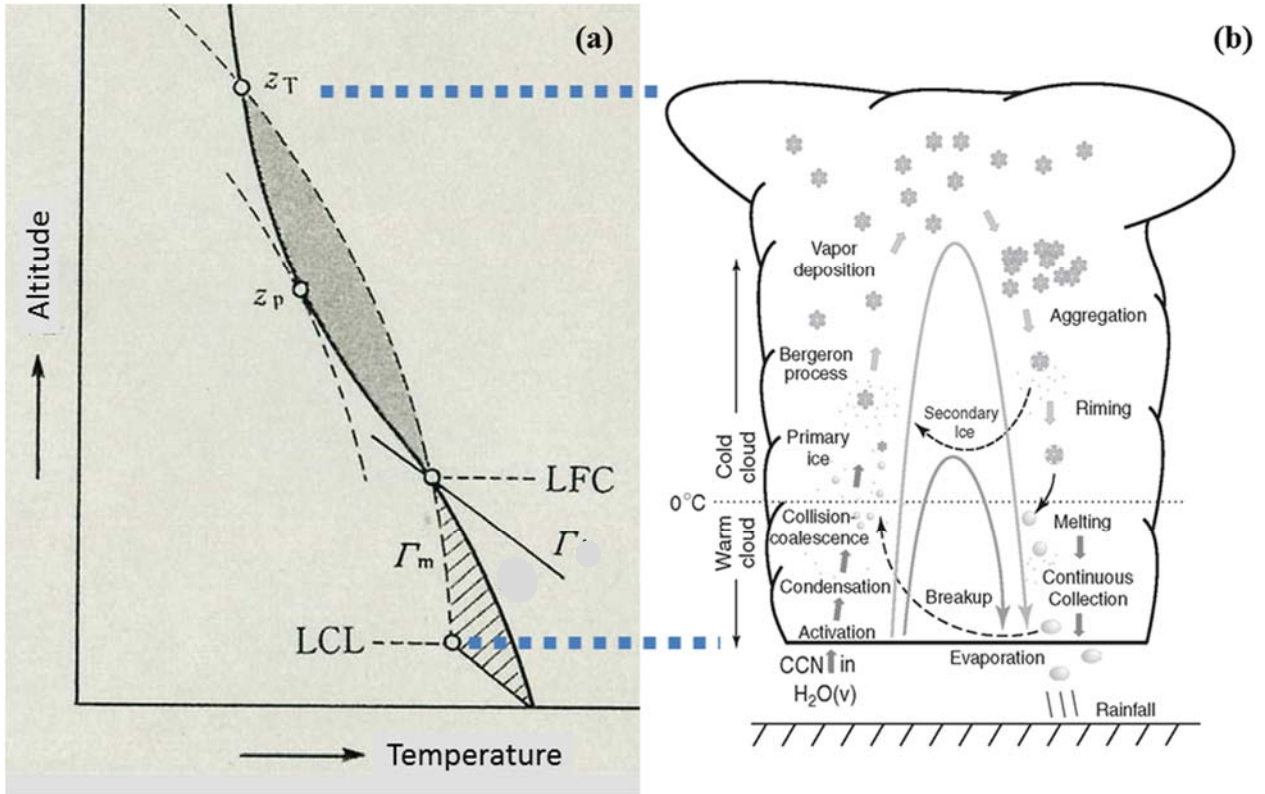


Fig. 6.14 Schematic pictures for typical convective cloud, concerning (a) temperature profile (thick curve) and (b) microphysical processes (Lamb, 2003).

vertical temperature gradient satisfies

$$-\Gamma < \frac{\partial T}{\partial z} < -\Gamma_m \quad \left(i.e., \quad \frac{\partial \theta}{\partial z} > 0 \quad \text{and} \quad \frac{\partial \theta_e^*}{\partial z} < 0 \right), \quad (6.32)$$

then the atmosphere is unstable and generates (vertical) convection as mentioned in the previous section, if a parcel is saturated (in a cloud). If not (below, outside and above of the cloud), the atmosphere is stable. This situation is called the *conditional instability*.

In general the tropical lower and middle troposphere satisfies (6.32), and at the tropopause $\theta \approx \theta_e \approx \theta_e^* \approx \theta_e(z = 0)$ (the left-hand side panel of Fig. 3.6). Even in the tropics, however, $\theta_e < \theta_e^*$ for large regions in the troposphere, so that an air parcel moves upward only in case of any forcing as the dry (unsaturated) process with keeping θ (exactly speaking, the virtual potential temperature θ_v corresponding to the virtual temperature T_v), that is decreasing T by the dry adiabatic lapse rate Γ as in (3.7). If the forcing to lift up the air parcel is continued enough to reach an altitude called the *lifting condensation level (LCL)*, where the moisture satisfies the saturation ($r = r_s$), then the condensation started and LCL becomes the cloud bottom. Furthermore, if the forcing is continued (because still T of the parcel at LCL is cooler than the surrounding atmospheric temperature), the parcel continues to move upward and condense the involved water vapor (to generate cloud droplets⁶¹) with keeping θ_e^* (of the value at the LCL), that is decreasing T by the slower moist adiabatic lapse rate Γ_m as in (3.11), and may reach an altitude called the *level of free convection (LFC)*, where T of the parcel becomes equal to the surrounding atmospheric

⁶¹This process is irreversible and diabatic, because all the cloud droplets are assumed to be removed from the parcel (and fall to the ground as raindrops) with taking out a very small amount of heat, and is called *pseudoadiabatic*.

temperature decreasing upward steeper than Γ_m in the conditionally unstable situation (6.32). After that the parcel (warmer than the surrounding atmosphere) may move upward without forcing, until losing the buoyancy at an altitude (that is the cloud top) where T becomes equal to the surrounding temperature again. At the tropopause, above which the surrounding temperature gradient is changed rapidly to positive in the tropics, most of clouds must have the tops there or below. Similarly at the so-called *inversion layer* over the trade wind on the tropical ocean (Section 4.1) and also on the Indochina peninsula before the monsoon onset (Nodzu et al., 2006), lower convective clouds have tops.

The moist process producing the latent heat occurs only in the updraft area of a cloud, whereas the dry adiabatic process under rather stable stratification appears in the (broader) downdraft area surrounding the cloud even in the tropics. Considering this fact and the saturation and thermodynamic equations, (2.7) and (3.10), may be rewritten as

$$\left(\frac{\partial}{\partial t} + u\frac{\partial}{\partial x} + v\frac{\partial}{\partial y}\right)\theta + \Gamma_e w \approx \frac{e^{(R/c_p H)z}}{C_p}(J + LS), \quad (6.33)$$

where $\Gamma_e \equiv \begin{cases} \theta \cdot \partial \ln \theta_e^* / \partial z & \text{for } r \geq r_s \text{ and } w > 0, \\ \partial \theta / \partial z & \text{for } r < r_s \text{ or } w \leq 0. \end{cases}$

Γ_e is called the *equivalent static stability*. If there are no radiative heating nor additional moisture input, the righthand-side of the rewritten thermodynamic equation (6.33) becomes zero. If we replace (6.5) and (6.7) by (6.33) (and rewrite θ by T appropriately), we may solve the governing equations for moist convections by the mathematically same manner (without using r as a variable explicitly) as for dry convection mentioned in the previous subsection. Therefore the basic features of the cloud convections should be similar to those of the Bénard-Rayleigh convections described in the previous subsection: generation governed by the critical Rayleigh number, aspect-ratio (vertical/horizontal scales) of approximately unity, and so on. For the tropical troposphere the vertical scale is restricted by the tropopause height around 17 km, the horizontal scale of the whole convection (combining both updraft (cloud) and downdraft (clear) areas) should be similar. Corresponding to the fact that the latent heating occurs only in the updraft area, the value of Γ_e is larger in the downdraft area than in the updraft area. Thus the updraft (cloud) is narrower and stronger than the downdraft (clear area). Numerical calculations including nonlinear and dissipation terms have simulated realistic lifetimes from 10 min to 1 h. The criterion (6.32) is conditional, so that convections are not always generated even if (6.32) is satisfied. However, if convections are generated, they may extend beyond the initial (lower-tropospheric) conditionally unstable layer and reach at above the tropopause. For details of these features, see textbooks on dynamics of convective clouds (e.g., Houze, 1993; Emanuel, 1994; much simpler descriptions are also given in Section 9.5 of Holton, 1992).

The *convective available potential energy (CAPE)* provides a measure of the maximum kinetic energy for a convectively unstable parcel, assuming that water vapor and condensed water do not affect the buoyancy, and also that the parcel ascends without mixing with the environment ($K' = 0$) and adjusts instantaneously to the local surrounding pressure ($\phi' = 0$). The left-hand side of the vertical momentum equation (6.3) for such a parcel is expressed by the Lagrangian time derivative as in (2.1)–(2.3): $\frac{Dw'}{Dt} = \frac{Dz}{Dt} \frac{dw'}{dz} = w' \frac{dw'}{dz} = \frac{d}{dz} \frac{w'^2}{2}$, and the right-hand side is only the buoyancy term $(R/H)T'$ where $H = R\bar{T}/g$. Therefore,

$$\text{CAPE} \equiv \frac{w'^2}{2} \Big|_{\text{max}} = g \int_{z_{\text{LFC}}}^{z_{\text{T}}} \frac{T'}{\bar{T}} dz, \quad (6.34)$$

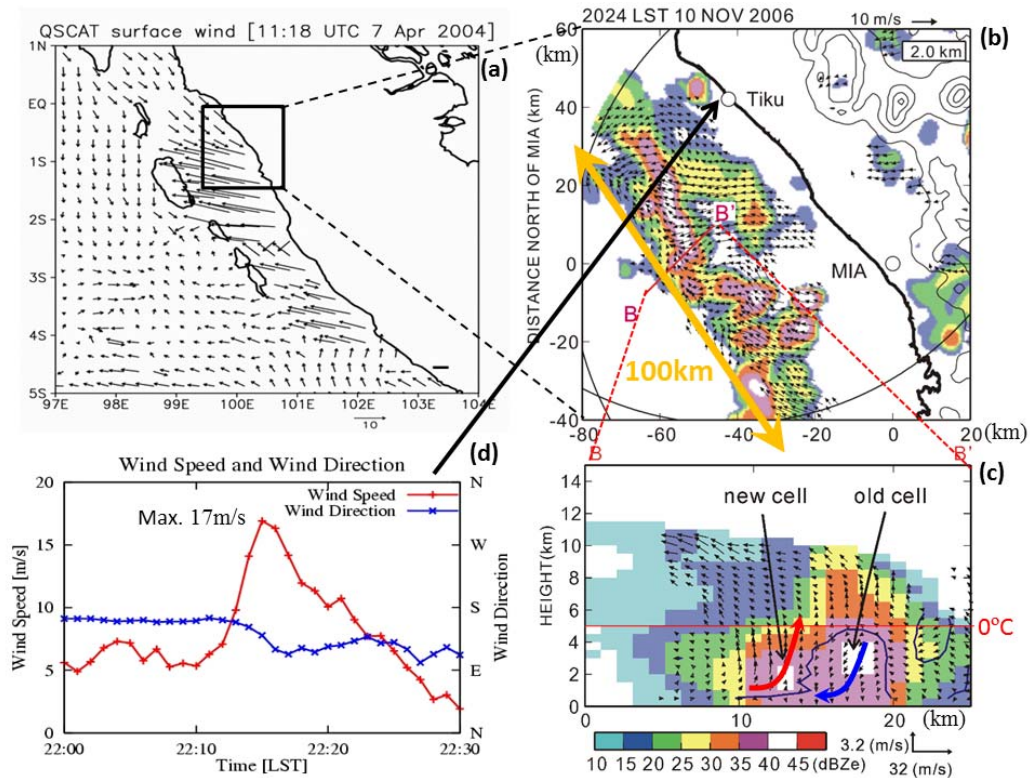


Fig. 6.15 Observations of development of a convective cloud system at (a) the western coast of Sumatra with other case of QuikSCAT sea-surface wind: (b) horizontal and (c) vertical displays of rainfalls (contours) and winds (arrows) observed with dual X-band Doppler radars installed at Tiku and MIA indicated in (b) (Sakurai et al., 2009, 2011), and (d) strong gust observed with surface anemometer (Kawashima et al., 2006, 2011).

where T' is given by the deviation of parcel temperature from the surrounding temperature \bar{T} , z_{LFC} is the altitude of LFC ($T' = 0$ there), and z_T is the other zero buoyancy level ($T' = 0$ again) around the tropopause (see the left panel of Fig. 3.6). For typical values $T' \approx 1-2$ K between $z_T - z_{LFC} \approx 10-12$ km over the tropical ocean, we have $CAPE \approx 500 \text{ m}^2/\text{s}^2$, which is smaller than the supercell (to be mentioned later) over the mid-latitude continent. Actually the scales of thundershowers (with graupels) and water spouts associated with cumulonimbus clouds observed in the maritime continent are generally smaller than thunderstorms (with hails) and tornadoes in the central US, although the generation frequency and total rainfall is larger in the former than in the latter.

Actual cloud is not vertically one-dimensional but three-dimensional, and ascending saturated air parcels inside the cloud may be mixed by the so-called *entrainment* of less moist or dry surrounding/outside air. Some cloud droplets are evaporated to maintain saturation of the parcels/clouds, and the latent 'cooling' due to evaporation reduces θ_e and w' of the parcels.⁶² Therefore the CAPE (6.34) overestimates the actual kinetic energy.

The mesoscale convective cloud systems (in any latitudes) are primarily categorized into the single cell, the multicell, and the supercell storm (with lifetimes of roughly 0.5 h, many hours and much longer, respectively⁶³), and their occurrences are mainly dependent on the vertical shear (roughly < 10 , $10-20$ and > 20 m/s, respectively, below 4 km altitude) (see e.g., Houze, 1993), which are not explained by the magnitude of CAPE. In the multicell storm, a *gust front* (with cold downdraft/outflow induced by raindrop evaporation) of the old cell makes the conditionally-

⁶²For more discussions on the entrainment, see Subsection 9.5.4 of Holton (1992) (for details, e.g., Houze, 1993; Emanuel, 1994).

⁶³For individual convective cell (cumulonimbus cloud) involved in a multicell the lifetime is similar to the single cell.

unstable surface air to ascend and generate the new cell. In the supercell the vertical shear makes the convection cell to tilt and slow development, which results in a very strong storm with tornadoes⁶⁴. Vertical shears in speed and in direction affect the most unstable modes, such as preference of rolls aligned in the shear flow direction (Asai 1972). To the present author's knowledge, there has not been any report of a supercell in the tropics, probably because of no broad plains. In the maritime continent Kawashima et al. (2006, 2011) and Sakurai et al. (2009, 2011) reported Doppler radar observations of cumulonimbus systems in west Sumatera.

The ice phase (ice crystals, snowflakes, graupels and hails) involved in the cumulonimbus cloud produces a strong local electric field, thunder and lightning. It was based on the thunderstorm frequency that Ramage (1968) named the maritime continent. Concerning lightning, Hidayat and Ishii (1998) analyzed seasonal and diurnal variations around Jawa, Hamid et al. (2001) showed ENSO impacts over the IMC, Kodama et al. (2006) showed lightning activation due to stronger convective instability in dry (El Niño) phase, and Virts et al. (2013a, b) studied Madden-Julian oscillation (MJO; see Section 6.4) and diurnal cycles based on a global network. They are in general consistent with the convective cloud activities described in this article, but more studies are needed for the significance of vertical (atmosphere-ionosphere) coupling and for a practical application to warn local torrential rainfall. Atmospheric electricity including thunderstorms may be another process linking atmosphere vertically.

In summary in the explanation mentioned above the following two aspects are important. One is the necessity of any mechanism to lift the surface air (with large θ_e) to the LCL and the LFC. The other is the mechanisms to organize the convective clouds (expected to be individually small-scale and distributed homogeneously) into large-scale structures as observed actually in the tropics. In the extratropics the geostrophic wind-pressure field has an instability mechanism to generate the extratropical cyclone-front systems, which produce large-scale updraft areas. In the tropics there are in total three phenomena/mechanisms to cause the conditional instability effectively. The first one has been described in Section 6.1 as the diurnal-cycle sea-land breeze circulations forced near the coastlines. The other two are developed by multi-scale destabilization mechanisms interacted/coupled with (water vapor supply from) the warm ocean water. In the subtropics, on one hand, somewhat apart from the equator the Coriolis force may work to produce a strong vortex, which is the tropical cyclone to be mentioned in Section 6.3. In the vicinity of the equator, on the other hand, a Matsuno-Gill pattern organized over the open ocean with interacting each other, which is the intraseasonal variation (such as MJO) travelling eastward along the equator (Section 6.4).

6.3. Conditional instability of second kind (CISK) and tropical cyclones

Yanai et al. (1973) proposed an evaluation method of the large-scale effect of clouds in the tropics with insufficient number of observations. The thermodynamic equation (2.5) and the water vapor conservation equation (the second one of (2.4)) are integrated for a large-scale horizontal area:

$$\left(\frac{\partial \bar{T}}{\partial t} + \bar{u} \frac{\partial \bar{T}}{\partial x} + \bar{v} \frac{\partial \bar{T}}{\partial y}\right) + \bar{w} \left(\frac{\partial}{\partial z} + \Gamma\right) = \bar{Q}_1 = \frac{\bar{J} + L\bar{S}}{C_p} - \frac{1}{\rho_0} \frac{\partial \rho_0 \bar{T}' w'}{\partial z}, \quad (6.35)$$

$$\frac{L}{C_p} \left(\frac{\partial \bar{r}}{\partial t} + \bar{u} \frac{\partial \bar{r}}{\partial x} + \bar{v} \frac{\partial \bar{r}}{\partial y} + \bar{w} \frac{\partial \bar{r}}{\partial z}\right) = \bar{Q}_2 = -\frac{L}{C_p} \left(\bar{s} + \frac{1}{\rho_0} \frac{\partial \rho_0 \bar{r}' w'}{\partial z}\right), \quad (6.36)$$

⁶⁴A line-shaped ensemble of multi- or super-cells is called the *squall line*, which moves in a different direction than the individual thunderstorms (similar to the equatorial supercluster; Section 6.4).

where $\overline{Q_1}$ and $\overline{Q_2}$ are the apparent heat source and moisture sink for the large-scale dynamics. Note $\overline{(\)}$ and $(\)'$ are *not* the zonal mean and disturbance, but the average for a regional (observed) area and an anomaly from this average. The moisture supply \overline{S} from the outside (ocean and land) does not appear explicitly, and is involved implicitly in the net condensation amount \overline{s} . At first each left-hand side can be calculated based on the large-scale observations (an objective analysis) of \overline{u} , \overline{v} , \overline{w} , \overline{T} and \overline{r} , which gives $\overline{Q_1}$ and $\overline{Q_2}$. Next the difference of each right-hand side of (6.35) and (6.36) becomes

$$\Delta\overline{Q} \equiv \left(\overline{Q_1} - \frac{\overline{J}}{C_p} \right) - \overline{Q_2} = -\frac{1}{C_p\rho_0} \frac{\partial}{\partial z} \rho_0 (C_p \overline{T'w'} + Lr'w') \approx -\frac{1}{C_p} \frac{\partial \overline{h'w'}}{\partial z}, \quad (6.37)$$

where h' is a perturbation of the *moist static energy*:⁶⁵

$$h \equiv C_p T + \phi + Lr, \quad dh \approx C_p T \cdot d \ln \theta_e. \quad (6.38)$$

Therefore the contribution by clouds $\partial \overline{h'w'}/\partial z$ can be evaluated from $\overline{Q_1}$, $\overline{Q_2}$ and the radiative heating \overline{J} as another calculable quantity, without knowing \overline{s} .

In the moist (pseudo-)adiabatic process ($\theta_e = \text{const.}$) h is approximately conserved, the integration of (6.37) in the cloud becomes

$$\int_{(\text{cloud bottom})}^{(\text{cloud top})} \Delta\overline{Q} dz \approx -\frac{1}{C_p} [\overline{h'w'}]_{(\text{cloud bottom})}^{(\text{cloud top})} \approx 0. \quad (6.39)$$

Observations confirmed (6.39), which implies that the effect of convective clouds is not negligible. Therefore the numerical model even for the large scale phenomena must express it ($\partial \overline{T'w'}/\partial z$, etc. in the original equations) in the tropics. In order to overcome this issue, there are two strategies: parameterization and high resolution. The former is to express small (sub-grid) scale phenomena by an experimental/theoretical formula, whereas the latter is to improve (zoom up) the spatial resolution (and time step). In the cloud process these are not separable, because the microphysical and turbulent process cannot be observed practically and calculated explicitly, and any parameterizations are inevitably necessary. These are not only technical issues of numerical calculation, but also theoretical issues on why/how multiple scale phenomena from microphysics to large-scale dynamics appear in the tropical atmosphere.

The most popular large-scale phenomena in the (sub)tropics are the *tropical cyclones*, which are called *typhoons* in the northwestern Pacific and *hurricanes* in around the north America. They are intense vortical storms that develop over very warm surface water the tropical oceans (except for around the south America). Their typical radial scales are several hundred kilometers, but the horizontal scale of the region of most intense horizontal winds is typically only about 100 km in radius. Because the Coriolis force needs to sustain strong *gradient* (mainly geostrophic plus partly *cyclostrophic*) tangential winds (50–100 m/s) with strong radial pressure gradient due to very low central pressure, they appear in general in the latitudes higher than around 10° (Fig. 6.16). This structure may be described by equations similar to the zonal mean global circulation (4.2)–(4.6), if we consider the northern hemisphere ($f > 0$) and take x -coordinate in the clockwise tangential direction along the circular isobar (pressure contour line), y -coordinate in the outward radial direction and z -coordinate in the upward vertical direction⁶⁶. In this case the

⁶⁵ h is the sum of the enthalpy $C_p T + Lr$ and the gravity potential energy ϕ , and also the sum of the dry static energy $C_p T + \phi$ and the latent heat Lr . When h is conserved, the integration of h from LFC to the cloud top is approximately equal to CAPE (6.34). Because h is approximately conserved when θ_e is conserved, h is used as an alternative to θ_e .

⁶⁶This local Cartesian description of the cylindrical coordinate system is different from more popular one (x : outward, y : ‘anti-clockwise’ tangential; z : upward) but is better for considering the similarity to the equatorial global case.

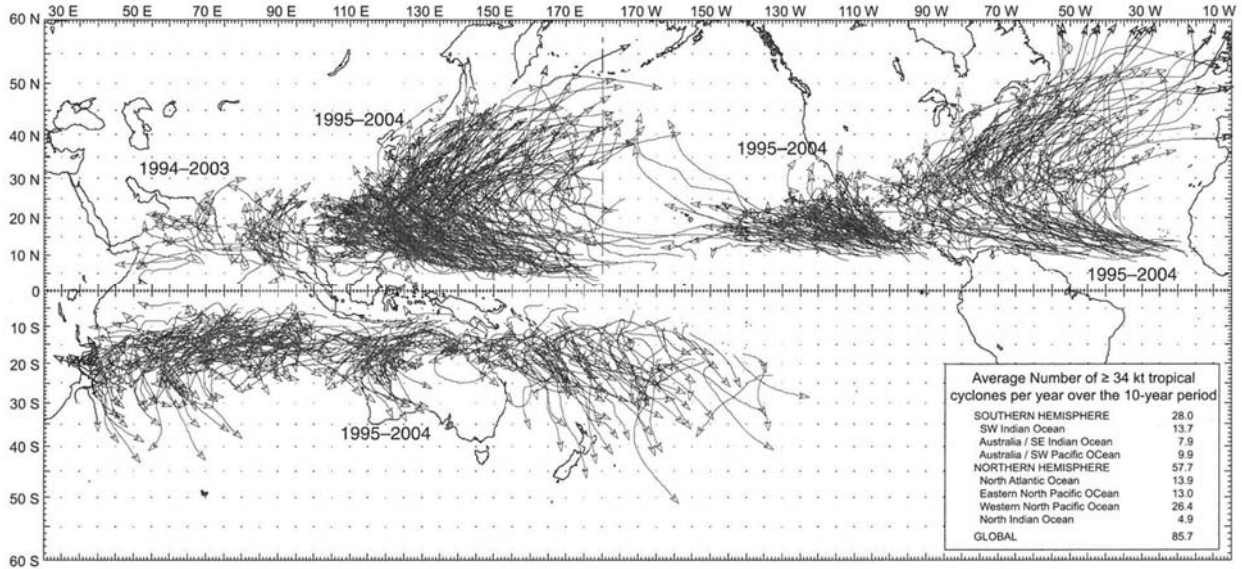


Fig. 6.16 Genesis locations and tracks of tropical cyclones (with winds ≥ 17 m/s) in 1995–2004 (Lin, 2007).

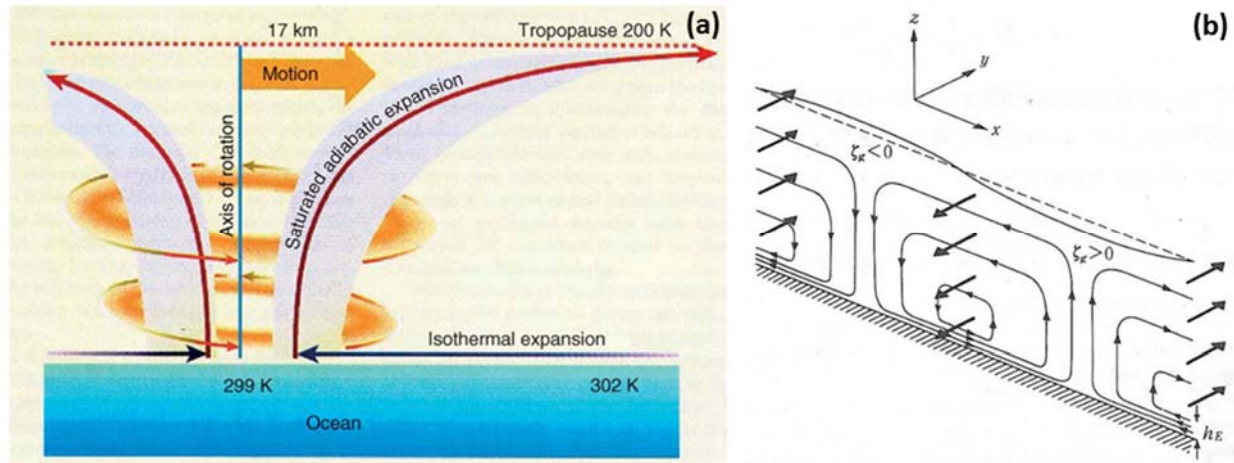


Fig. 6.17 Schematic figures of (a) the ‘meridional’ (secondary) circulation (Willoughby, 1999), and (b) the Ekman pumping (Pedlosky, 1979) of the tropical cyclone.

tangential wind is anti-clockwise ($\bar{u} < 0$) for the northern hemisphere ($y > 0$), and clockwise ($\bar{u} > 0$) for the southern hemisphere ($y < 0$). The Coriolis factor f should be replaced by $f + \bar{u}/y$ including the centrifugal force. Considering that the angular momentum $M = (f/2)y^2 + (-\bar{u})y$ is conserved, the tangential wind $\bar{u} = (f/2)y - M/y$ becomes a monotonically increasing (cyclonically decreasing) function of y , the cyclonic rotation ($\bar{u} < 0$) is limited for $y < \sqrt{2M/f}$. Actual typhoon suggests $\sqrt{2M/f} \sim$ a few hundreds of km. In order to settle M and \bar{u} near the center as realistic values, f should be sufficiently large, which requests the latitude larger than about 10° .

The ‘meridional’ (radial-vertical) circulation (\bar{v} , \bar{w}) (Fig. 6.17(a)) may be considered by applying the case of Hadley circulation (4.20) or (4.23) (with replacing f by $f + \bar{u}/y$). In the boundary layer \bar{u} has the opposite sign to both $f + \bar{u}/y$ and the x -direction friction \bar{G} , thus the radial wind must blow to the center ($\bar{v} < 0$). By the conservation of M , the centrifugal force \bar{u}^2/y increases rapidly with approaching to the center ($y \rightarrow 0$), and exceed the y -direction pressure gradient completely, which implies that air cannot enter into the vicinity of the center ($\bar{v} \rightarrow 0$) if the acceleration term is not neglected, and the continuity equation (similar to (4.5) in the zonal-mean case) requests very large updraft $\bar{w} > 0$, which is sustained by very large \bar{Q} due to the very active (very strongly latent

heating) convective clouds. Namely, reading the second formula of (4.20) inversely:

$$\bar{Q}(\approx \bar{Q}_1) \approx \Gamma \cdot \bar{w}, \quad (6.40)$$

we expect the temperature lapse rate Γ or the updraft \bar{w} must be parameterized appropriately in order to construct a numerical model of typhoon/hurricane. Inside this no updraft (clouds) and the vorticity conservation ($\partial(-\bar{u})/\partial y = \text{const.}$) requests decrease of \bar{u} toward the center⁶⁷. These structure in the vicinity of the tropical cyclone center is called the *eye*, and the very tall clouds surrounding it are called *eye wall* (Fig. 6.18).

A parameterization of Γ has been mentioned as the convective adjustment (Manabe and Strickler, 1964) in Section 3.2: if the calculated lapse rate $-\partial T/\partial z$ in an altitude region exceeds a critical value⁶⁸, it is rewritten by T satisfying $\theta_e = \text{const.}$ and no change of the energy before and after the adjustment (therefore (6.39) holds automatically). This scheme is, however, cannot express the large-scale effect of cumulus clouds growing beyond the unstable layer top as pointed out in the previous section. Kuo (1974) proposed a formula similar to the Newtonian cooling (3.6)⁶⁹:

$$\bar{Q} - \frac{\bar{J}}{C_p} \approx -\alpha(\bar{T} - \bar{T}_c) \quad \text{for} \quad z_{(\text{cloud bottom})} \leq z \leq z_{(\text{cloud top})}, \quad (6.41)$$

which makes relaxation to a standard temperature profile \bar{T}_c in the cumulus (e.g., given by the moist pseudoadiabatic lapse rate based on θ_e at the cloud bottom (LCL)) by a finite time given by α^{-1} . This scheme can express the heating effect up to the cloud top (where actual \bar{T} is identified with the value in the moist pseudoadiabatic profile) much higher than the initial unstable layer top. The relaxation time constant α has, however, very broad arbitrariness (even within the condition (6.39)).

Ooyama (1969) noted the updraft (moisture flux) inside a cloud over the convergence of moist air in the planetary boundary layer, and proposed another parameterization:

$$\bar{Q} - \frac{\bar{J}}{C_p} \approx \eta \cdot \frac{\rho_{(\text{boundary layer top})}}{\rho_0} \frac{\partial \bar{\theta}}{\partial z} \cdot \bar{w}_{(\text{boundary layer top})} \quad \text{for} \quad \bar{w}_{(\text{boundary layer top})} > 0 \quad (6.42)$$

In this case the non-dimensional parameter η is essentially important. Under the condition (6.39), if $\eta > 1$, then $\bar{w}_{(\text{inside cloud})} > \bar{w}_{(\text{boundary layer top})}$, implying the existence of entrainment effect due to mixing of outside air to the ascending air inside the cloud. $\bar{w}_{(\text{boundary layer top})}$ can be obtained by applying the wind-driven ocean equations (5.24) for the boundary layer-driven free-atmosphere (perturbation from the axi-symmetric field) in the present problem. Replacing the Coriolis factor βy by constant f for simplicity, making $\partial(2\text{nd eq})/\partial x - \partial(1\text{st eq})/\partial y$ of (5.24), we have

$$\frac{\partial v'_{(\text{free atmosphere})}}{\partial x} - \frac{\partial u'_{(\text{free atmosphere})}}{\partial y} \approx -\frac{\alpha'}{f} \left(\frac{\partial u'_{(\text{boundary layer})}}{\partial x} + \frac{\partial v'_{(\text{boundary layer})}}{\partial y} \right). \quad (6.43)$$

Because the inside of bracket in the right-hand side is the horizontal convergence in the boundary layer, (6.43) is rewritten by (5.5) as $+(\alpha'/\rho_0 f) \partial \rho_0 w'/\partial z$, which is approximated by $w'_{(\text{boundary layer top})}/$

⁶⁷Ishihara et al. (1986) and Tabata et al. (1992) by meteorological Doppler radars and Shibagaki et al. (2003) and Teshiba et al. (2005) by wind profilers showed detailed structures of typhoon eyes, and Fudeyasu et al. (2008a) showed the origin of rainwater near a typhoon eye, although they were all in the mid latitudes (Japan).

⁶⁸This is a measure of generation of convection, formulated for example to take a value between Γ_m and Γ as a function of the relative humidity r/r_s .

⁶⁹A similar parametrization (usually with a different value of α) is applied also for \bar{Q}_2 concerning r .

(boundary layer depth), since $w' = 0$ at the bottom (sea surface). Because the left-hand side is the perturbation of vertical vorticity in the free atmosphere (of which the axi-symmetric component is given by a formula similar to (4.18)), the meaning of (6.43) is that the cyclonic/anticyclonic vorticity in the free atmosphere is on the up-/down-draft in the boundary layer (Fig. 6.17(b)), which is called *the Ekman pumping*.

By the Ekman pumping mechanism, the tropical cyclone as a very strong cyclonic vortex may be associated with many very strong updraft areas in the boundary layer. In the conditionally unstable atmospheric boundary layer over the tropical ocean, in particular over very warm water of the tropical western Pacific⁷⁰, the updrafts become cumulus convections developing beyond LFC and their released latent heat sustain (through \bar{Q}) the tropical cyclone-scale \bar{w} . This process is expressed, by x -averaging (6.43) and using (6.42), as

$$\bar{w}_{(\text{boundary layer top})} \approx -\frac{fd}{\alpha'} \bar{q}, \quad \bar{w}_{(\text{vortex top})} \approx \eta \cdot \bar{w}_{(\text{vortex bottom})}, \quad (6.44)$$

where $d \approx \sqrt{K'/f}$ is the boundary layer depth (similar to the Ekman layer depth δ_E (6.25)), and the Rayleigh damping factor in (6.43) has been rewritten as $\alpha' \approx K'/d^2$ by the eddy diffusivity K' . Taking y -differentiation of the tangential momentum equation similar to (4.2)⁷¹, using the axi-symmetric continuity equation similar to (4.5), and z -integrating from the free-atmosphere bottom (the boundary layer top) to the vortex top (height: H), we obtain

$$\frac{\partial \bar{q}}{\partial t} \approx -f \frac{\partial \bar{v}}{\partial y} = f \frac{\partial \bar{w}}{\partial z} \approx \frac{f}{H} [\bar{w}]_{(\text{boundary layer top})}^{(\text{vortex top})} \approx (\eta - 1) \frac{\sqrt{K'/f}}{H} f \bar{q}. \quad (6.45)$$

Therefore, if $\eta > 1$, the vorticity \bar{q} increases in time, and the vortex is developed, and the inverse of the factor of \bar{q} in the right-hand side, $H/[(\eta - 1)\sqrt{K'f}]$, is called the *spin up* time. The latent heat \bar{Q} released by cumulus clouds make \bar{w} (> 0) and (by the continuity) \bar{v} (< 0) increase, by which air moved toward the center make (by conservation of M) the cyclonically rotating tangential wind $-\bar{u}$ and its gradient-balanced pressure gradient $\partial \bar{\phi}/\partial y$ increase (that is, the central minimum pressure deepen). The cyclonic development in this way is feedback to the enhancement of w' , that is the cumulus cloud development at the beginning. This theoretical mechanism may explain the realistic development time scale and the dominant horizontal scale of actual typhoons and hurricanes, and Charney and Eliassen (1964) had named this mechanism as the *conditional instability of the second kind (CISK)*. An improvement considering an initial role of wave disturbance to make convergence and local instability has been also proposed (Hayashi, 1970; Lindzen, 1974).

Energetically speaking, the kinetic energy of a tropical cyclone is always dissipated in the boundary layer and supplied by the conversion of latent heat obtained by ocean surface evaporation, through the potential energy producing the 'meridional' circulation. Increasing the surface (mainly tangential) wind speed, the sea surface disturbance, evaporation and latent heat supply are enhanced much more, and the boundary-layer inflow \bar{v} , θ_e and a potential energy making feedback to the tangential wind \bar{u} increase rapidly from outside to inside. This mechanism is called the *wind-induced surface heat exchange (WISHE)* (Emanuel, 1987; Neelin et al., 1987). In the narrow outward-sloping eyewall clouds throughout the troposphere, air may ascend without forcing, because both θ_e and M are conserved along the updraft, which is neutral in the meaning of the (conditional) symmetric stability mentioned in Section 4.3. Radial outflow exists in a rather thin layer near the tropopause, and rather weak downdraft

⁷⁰Observations suggest that the tropical cyclones are generated/developed over the ocean surface water warmer than about 26.5°C.

⁷¹We may neglect $\partial \bar{u}/\partial y$ (in comparison to f), $\partial \bar{u}/\partial z$ (by the nature of vortex tending to be parallel to the rotating axis; the Taylor-Proudman theorem), and \bar{G} (without considering any systematic distribution of clouds).

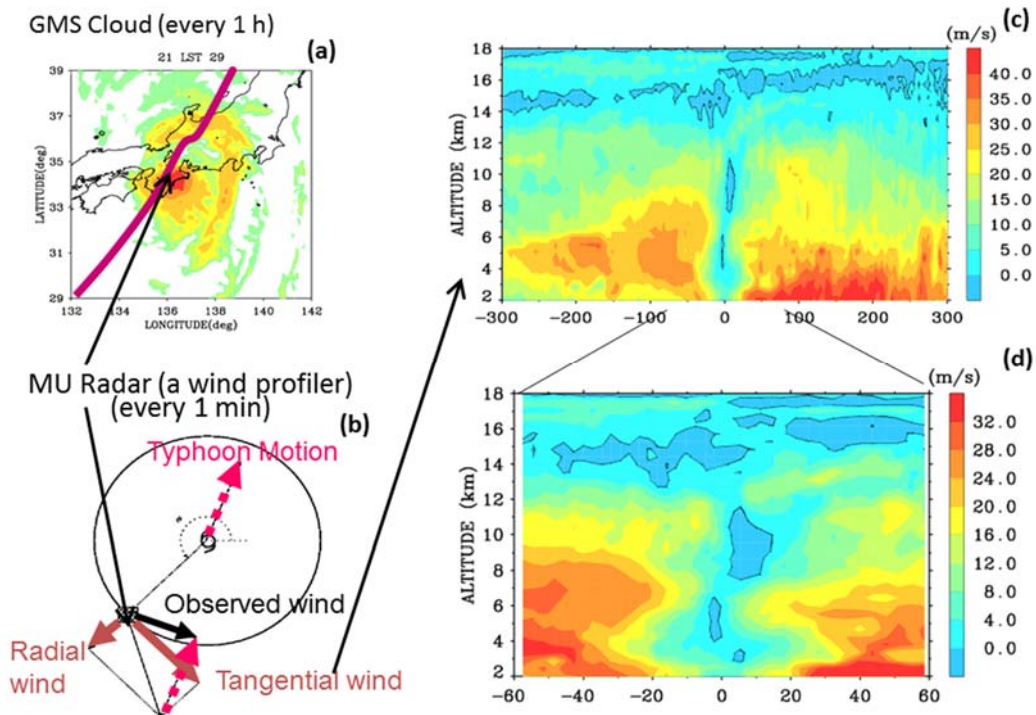


Fig. 6.18 Wind profiler (MU radar) observation of (a) a matured typhoon (T9426, Orchid) just passed by. (b) Subtraction of the moving velocity from the observed wind velocity, and decomposition between the radial and tangential wind components. (c) Pseudo-‘meridional’ cross-section (with radial distance exchanged from time series at the single observatory; positive is the foreside) of the tangential wind velocity and (d) its magnified one showing the ‘eye’ structure. After Shibagaki et al. (2003).

region is distributed broadly. With this structure the tropical cyclone is warmer than the surroundings, which is called the *warm core*.

Because the typhoons in Asia-Pacific countries, the hurricanes in north-central American countries and others (the cyclones in south Asian and southern Pacific countries) are still of the worst meteorological disasters, improvement of numerical prediction (and warning/informatics of the prediction products) of the tropical cyclones is one of the biggest issue in the meteorological operations, although almost real time tracking of the center and storm (torrential rain and/or violent wind) distribution of each cyclone has been achieved so much by the meteorological satellites and radars. The movement of tropical cyclone of mesoscale follows the large-scale wind field, so that the latter is quite important for prevention of the typhoon/hurricane disasters and have been improved very much during these decades. Prediction of development/decay of the tropical cyclone is just that of cumulus clouds, namely parameterization or high resolution as mentioned in the previous section. The physically most advanced parameterization was originated by Arakawa and Schubert (1974) who formulated the effect of subgrid-scale cumulus cloud activities by a function (types with the number of vertical levels) of the ‘entrainment ratio’ (corresponding to the cloud top height and η), and statistical features of each type of clouds under an energetical equilibrium.

For the weather forecast and disaster prevention each national operational agency defines categories of tropical storms, mainly based on the maximum wind speed near the center, and give a number or a name satisfying a definition. For example the Japan Meteorological Agency (and its leading Regional Specialized Meteorological Center Tokyo-Typhoon Center for the east Asia-Pacific region) defines a typhoon by its location in the northwestern Pacific and its maximum (10 min-averaged) wind stronger than 34 knot (≈ 17 m/s), and gives it a number restarting every year and an international name listed by WMO: <http://www.jma.go.jp/jma/jma-eng/jma-center/rsmc-hp-pub-eg/tyname.html>.

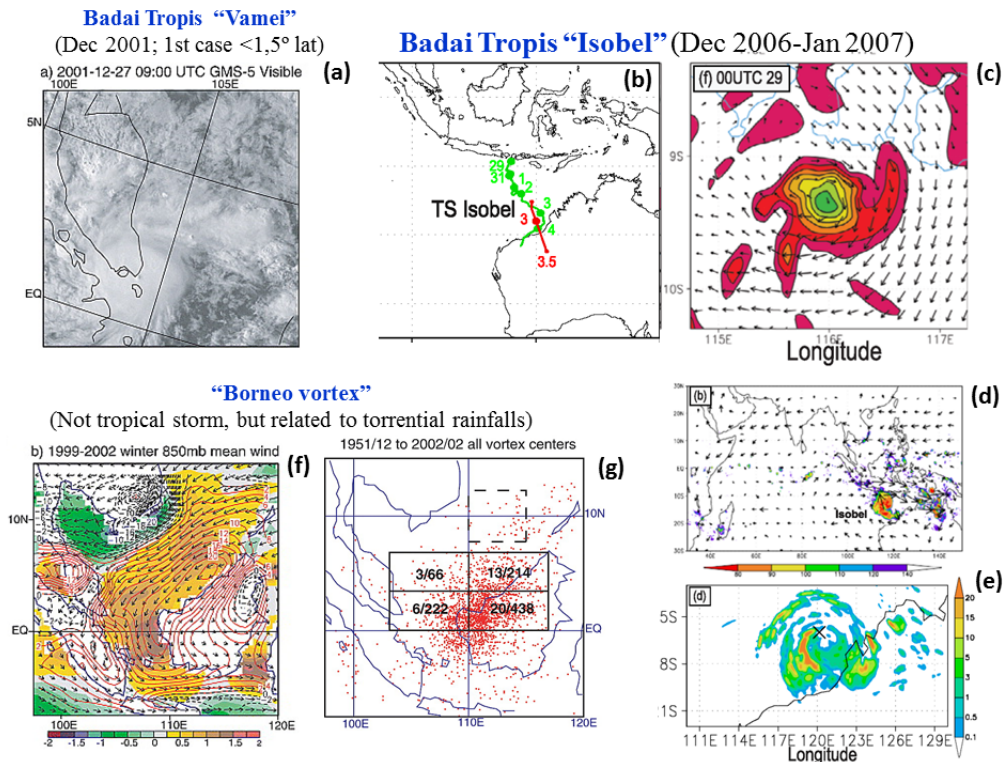


Fig. 6.19 Near-equatorial tropical cyclones: (a) *Vamei* (Chang et al., 2003), and (b)–(e) *Isobel* (Fudeyasu et al., 2008b). (f) – (g) Other sub-synoptic-scale vortical disturbances called “Borneo vortex” (Chang et al., 2003).

Details and differences in each country are mainly for disaster prevention rather than based on physics, and are not described in this text. Recently the increase and intensification of tropical storms interest the society, as a possible result by the global warming (e.g., Chan and Liu, 2004; Emanuel, 2005; Webster et al., 2005; Oouchi et al., 2006), although the societal vulnerability and damages are not dependent only on the physical characteristics of meteorological phenomena.

Because of the necessity of the Coriolis force, average annual occurrence of tropical cyclones inside the equatorial deformation radius (4.21) is only two (dispersed between zero and seven each year) on the northern (Philippine and Micronesian) side (during the past century; Kubota and Chan, 2009; Kubota et al., 2012; Kubota, 2012) and less than 1.5 on the southern (Australian) sides (for the last two decades of the last century; Hall et al., 2001). They are much rarer (as reported by Chang et al., 2003; Fig. 6.19(a))⁷² and not so much developed over inland seas and islands of the IMC (called “*badai tropis*” in Indonesia-Malay language), which could be simulated by high-resolution (cumulus-resolving) numerical models (Fudeyasu et al., 2008b) (Figs. 6.19(b)–(e)). Because the ITCZ shifts annually but is not completely following a weak annual cycle of solar radiation (Fig. 4.5), and it concerns typhoon generation mainly in the northern subtropics (often northern than 20°N in boreal summer), otherwise it involves mainly ISVs (because southward shifts of the ITCZ are not so deep even in the austral summer). However, a few very strong typhoons (such as a case and a “super typhoon” Haiyan (Yolanda, T1330) in 2013, as well as

⁷²There is another category of sub-synoptic-scale vortical disturbance (called the *Borneo vortex*, or *cold surge vortex*) appearing on around the South China Sea (e.g., Chang et al., 2003; Yokoi and Matsumoto, 2008; Tangang et al., 2008; Chen et al., 2015), considered to be developed by the stretching of vorticity due to updraft generated by latent heat release near the center and a rainband-like structure in the north east of the center. This category is related to, rather than a tropical cyclone, intensification of the cold (monsoon) surge (Section 4.4) and a cause of torrential rainfall in this area.

another one in 1912 almost just 100 years ago, and less strong ones such as reported by Holliday and Thompson, 1986, between them almost every about three decades) have been generated and developed very much along (for a few days a little southern than) 10°N (Kubota, 2014, private communications) . On the other hand, even near the South America with cool sea water, recent warming may produce a tropical cyclone (Pezza and Simmonds, 2005).

After landing the tropical cyclone decays gradually, because of losing the moisture supply and of increasing the friction at the bottom surface. This *spin down* process may be expressed by (6.45) with $\eta = 0$, and the decaying time scale is given by $H/\sqrt{K'f} \sim 1$ day. The frictional contrast between sea and land surfaces also makes low-level divergence and downdraft of upper air with large vorticity in the area with wind blowing from land to sea (e.g., in the western side for landing on a west-east coastline in the northern hemisphere), which makes a shift of the cyclone center as a cause of ‘freak’ tropical cyclone just before landing⁷³. After decaying some tropical cyclones become extratropical cyclones and develop again. For further reading on the tropical cyclones see convection and cloud dynamics textbooks (e.g., Houze, 1993; Emanuel, 1994), and also a recent project overview (Moncrieff, et al., 2012).

6.4. Multiple-scale cloud clusters and intraseasonal variations (ISVs): Madden-Julian oscillation (MJO)

(i) Observations

Takayabu and Nitta (1993) classified the tropical cloud clusters organized over the tropical ocean into two categories: one is the tropical cyclones with vortical shape generated way from the equator and moving with the large-scale within a limited region (such as over the northwestern Pacific and east Asia) flow for one to few weeks until decaying, which have been described in the previous section; the other is the *intraseasonal variations* (ISVs) to be described in this section, which are generated just as the Matsuno-Gill pattern-like shape (Figs. 5.8 and 5.9) and moving always eastward along the equator over an ocean or occasionally through the oceans for weeks to two months. The most dominant mode of ISVs was observationally discovered by Madden and Julian (1971, 1972), and is called the Madden-Julian oscillation (MJO), Nakazawa (1988) showed the *hierarchical structure* of MJO with a *super cluster* (with horizontal scale $\gtrsim 10^3$ km) involving smaller-scale *clusters* ($\sim 10^2$ km) of individual clouds ($\lesssim 10^1$ km), and that the smaller clusters move in a different (often opposite) direction from the super clusters (Fig. 6.20). As schematically shown in Fig. 6.21, the MJO super cluster starts developing with a surface low-pressure anomaly and boundary-layer moisture convergence over the Indian Ocean, warming and anomaly (Walker-like) circulation of the troposphere, and ascending of the tropopause. The system moves gradually eastward at about 5 m/s (~ 430 km/day, corresponding roughly to period of 1, 1.5, or 3 months for zonal wavenumber 3, 2 or 1, respectively) and becomes most active over the western Pacific. After reaching the central Pacific cooler than the western warm pool, the system gradually weakens, although occasionally anomaly continues to move more eastward around the globe (Takayabu et al., 1999). The MJO is like a Matsuno-Gill pattern consisting of equatorial Kelvin and Rossby waves (see Section 5.2), and its smaller hierarchies are likely to mixed-Rossby gravity or inertio-gravity waves.

Wheeler and Hendon (2004) originated the real-time multivariate MJO (RMM) index, based on a pair of empirical orthogonal functions (EOFs)⁷⁴ of the normalized daily anomalies of lower-/upper-level (850-/200-hPa) zonal wind and cloud top height (by outgoing longwave radiation). The principal components (RMM1 and 2,

⁷³Even over the ocean a tropical cyclone trajectory becomes irregular by weak large-scale wind, and by interactions of two cyclones approaching each other. The latter is called the *Fujiwhara effect* (Fujiwhara, 1923).

⁷⁴A comprehensive explanation (with simple examples) of the EOF analysis is given in Chapter 21 (pp.821–823) of Stull (2015).

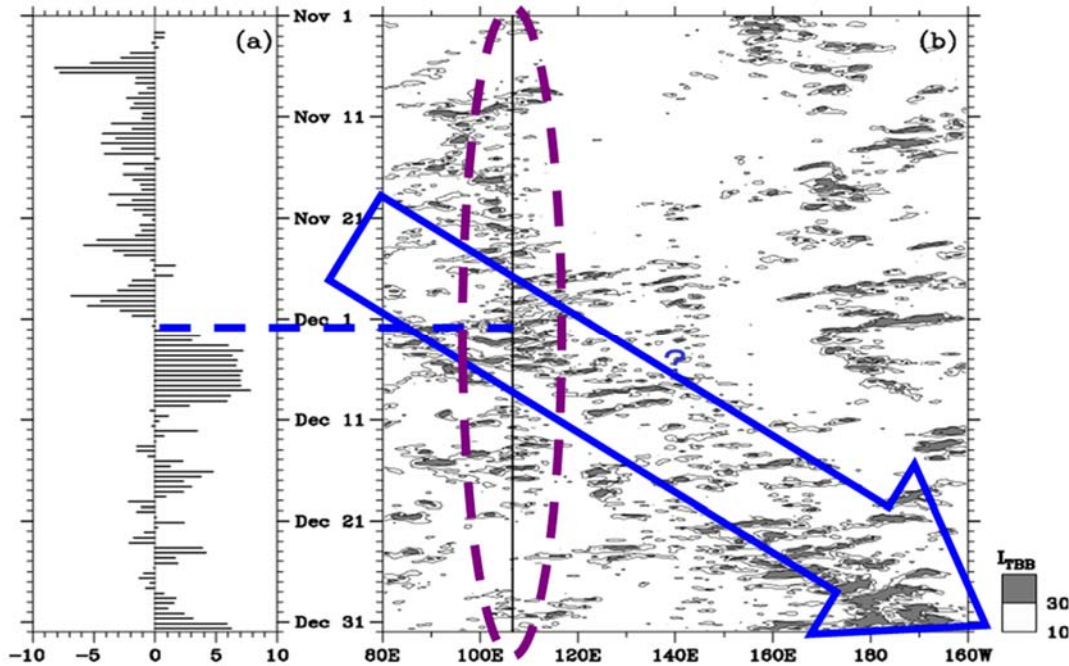


Fig. 6.20 An ISV passage detected by (a) wind profiler-observed (6°S , 107°E) semi-daily-mean lower-tropospheric zonal wind and (b) 3-hourly meteorological satellite-observed $I_{\text{TBB}} = 250 \text{ K}$ - black body temperature along 6°S (Hashiguchi et al., 1995a). As found in earlier studies, there is an eastward moving supercluster (the large arrow) and smaller hierarchies moving different directions. In addition, near the Jawa Island (the vertical line at 107°E in (b)) the diurnal cycles appeared clearly.

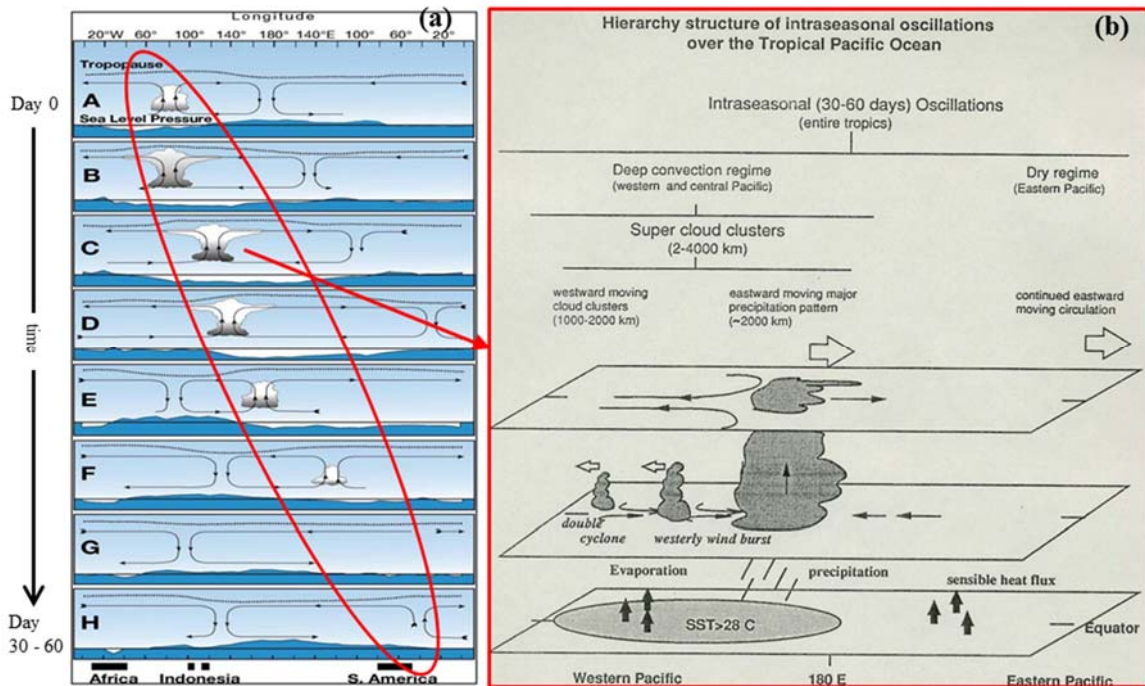


Fig. 6.21 Schematic figures of the Madden Julian oscillation (MJO): (a) eastward movement and longitudinal dependency (Madden and Julian, 1994) and (b) the internal hierarchical structure (Lau et al., 1989).

corresponding to temporal amplitude variations) of the first two leading functions (EOF1 and 2, corresponding to zonal convection distributions active near the IMC and inactive over the Indian Ocean, respectively)⁷⁵ are calculated and plotted in the RMM1-RMM2 plane (Fig. 6.22(a)–(c)). The MJO amplitude is given by the distance from the

⁷⁵The fact that the leading functions have not essentially changed since 1970s indicates the regularity of the MJO.

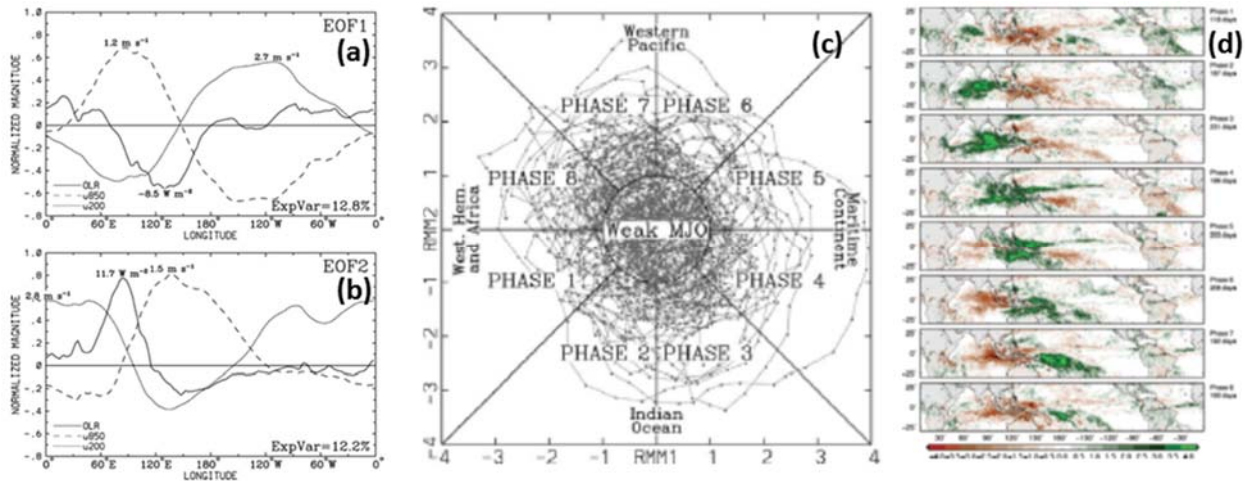


Fig. 6.22 (a)(b) The first two EOFs (see text) and (c) the real-time multivariate MJO (RMM) index space indicating eastward movement of MJO (Wheeler and Hendon, 2004). (d) Composites of intraseasonal (30–90 days) anomalies in TRMM precipitation (mm/day) during November–April of 1998–2012 based on the RMM index (Zhang, 2013).

origin, and if it is less than 1 (the amplitude less than the standard deviation), we define that MJO is weak. The MJO phases are defined (classified into 1–8) by the azimuthal location, which rotates usually anticlockwise. For example, if plotted near the bottom (RMM2 taking *minimum*), the convection center is located over the Indian Ocean, which is defined as phases 2–3. When plotted in the right (RMM1 taking maximum), the convection center is located near the IMC, which is defined as phases 4–5. Composites of this analysis for the boreal winter (Fig. 6.22(d)) show clearly that the convection center starts over the Indian Ocean, passes through the IMC and into the western Pacific, although more eastward propagation (go-around) is less clear. For the boreal summer, the MJO moves also northward due to monsoon (Lawrence and Webster 2002), which cannot be shown in the Wheeler-Hendon RMM index concerning only zonal movement. However, this index is recognized most useful to express MJO status, and calculated/reported operationally every day by Australian Bureau of Meteorology: <http://www.bom.gov.au/climate/mjo/>, and other countries' agencies also use this.

The MJO is considered to interact atmospheric/climatological phenomena from the diurnal cycle to interannual variability (Moncrieff et al. 2012). The MJO influences on almost global weather and climate through tropical cyclone activities (e.g., Liebmann et al. 1994; Maloney and Hartmann 2001) (Section 6.3), variations of teleconnections (Fig. 5.10), monsoons (e.g., Yasunari, 1979; Takeda and Ikeyama, 1984; Lau and Chan, 1986; Hendon and Liebmann 1990; Wang and Rui, 1990; Sui and Lau, 1992; also see a book edited by Lau and Waliser, 2005) (Section 4.4), ENSO/IOD (e.g., Nitta and Motoki 1987; McPhaden, 1999) (Section 5.3), the Indonesian throughflow (e.g., Gordon, 2005).

Because the MJO is a movement of the tropical convection center from the Indian Ocean into the Pacific, it influences regional weather and climate greatly in particular over the IMC in between. The rainy season onset of the southern hemispheric part of the IMC (Section 4.4) is determined by an ISV (Hashiguchi et al., 1995a) (see Fig. 6.20), and through the rainy season rainfall over the IMC increases actually during the active/wet phase of the dominant mode (MJO) of ISVs (Murata et al., 2002, 2006; Shibagaki et al., 2006a, b; Seto et al., 2006; Johnson and Ciesielski, 2013; Marzuki et al., 2013), in particular on surrounding seas larger than on the large islands (Hidayat and Kizu, 2009). Shorter hierarchy resembling mixed Rossby-gravity and/or inertio-gravity waves with periods of a few days also has been observed mainly near the eastern/western ends (Pacific and Indian Ocean sides) of the IMC (Takayabu

et al., 1996; Widiyatmi et al., 1999, 2001). The smaller-scale diurnal cycle rainfalls may be modified by larger-scale ISVs (Hashiguchi et al., 1995; Widiyatmi et al., 1999, 2001; Murata et al., 2002, 2006; Shibagaki et al., 2006; Rauniyar and Walsh, 2011; Kanamori et al., 2013; Peatman et al., 2014), seasonal cycle/monsoons (Hashiguchi et al., 1995; Renggono et al., 2001; Hamada et al., 2002; Okamoto et al., 2003; Sakurai et al., 2005; Xie et al., 2006; Araki et al., 2006; Koseki et al., 2013). Such modification/interaction may amplify diurnal cycles (Section 6.1) and cause heavy rainfalls in the western IMC (Wu et al., 2007, 2013).

Simultaneously the existence of the IMC influences the structure and movement of MJO quite largely. Based on satellite cloud cluster observations and objective analysis for about one year, Nitta et al. (1992) pointed out modification (such as propagation in the southern side of the equator) of the ISVs. Using more systematic analysis of longer-year data, essentially similar results are also confirmed recently by Zhang and Ling (2017). Mori et al. (2004), Wu et al. (2009b) and Ogino et al. (2016) have demonstrated the sea-side dominance of diurnal-cycle rainfall as CHeR (see Section 4), which is consistent with other evidence by Hidayat and Kizu (2009) that the ISV-correlated rainfall is also heavier than on the sea side. Locally roughly closed water cycle and a little opened energy release over the IMC are consistent with most of ISVs (super cloud clusters) decaying/modifying after landing the IMC. Cloud systems involved/maintained in an ISV migrating eastward over the Indian Ocean are decayed by almost complete consumption of water for rainfall in the local evening followed by clear atmosphere in the local morning. In this process the local rainfall keeps the diurnal cycle but its amount may be affected by moisture, stratification stability and wind field associated with the ISV. Therefore the diurnal cycle may be amplified by ISVs and, in longer time scale, by the annual cycle of the ITCZ (Sakurai et al., 2005; Wu et al., 2007, 2013).

The MJO/ISVs are phenomena mainly over the open ocean, and need special observations because there are no dense observations (islands themselves are not so many in particular over the Indian Ocean). The fully-operated (land, vessel, and space) scientific observation project focused on the MJO was started in 1992 over the western Pacific (Webster and Lukas, 1992; Nakazawa, 1995) and in 2006 over the Indian Ocean (Yoneyama et al., 2008, 2013).

(ii) Theoretical and numerical approaches

As mentioned in Chapter 5, there are various atmospheric waves in the tropical trade wind (easterly) zone. In the dawn of tropical meteorology based on physics and observations about half a century ago, studies on the stability of the axi-symmetric easterly to generate such *easterly wave* were done, following successful results on the mid-latitude westerly waves (baroclinic instability on the extratropical cyclones). However, the tropical atmosphere is *barotropic* (original meaning is ρ is a function only of p , and thus T is constant horizontally) and no vertical shear by the thermal-wind relation (4.11), that is, the dynamics becomes horizontal and two-dimensional. In this case the equatorial wave equation (5.9) may be written, with assuming $|m| \rightarrow 0$, $H \rightarrow \infty$ and $|\hat{\omega}| \ll N$, and recovering the horizontal shear term $\partial \bar{u} / \partial y$,

$$\frac{d^2 \tilde{v}}{dy^2} - \left(k^2 + \frac{k \tilde{\beta}}{\hat{\omega}} \right) \tilde{v} = 0, \quad (6.46)$$

where

$$\tilde{\beta} \equiv \frac{d\bar{q}}{dy} = \beta - \frac{d^2 \bar{u}}{dy^2} = \beta + \frac{1}{k} \frac{d^2 \hat{\omega}}{dy^2} \quad (6.47)$$

is the meridional gradient of the vertical vorticity and often called the *effective* β . (6.47) has a neutral solution (with a real ω) corresponding to the (barotropic) Rossby wave.

When $\beta = 0$, namely $\tilde{\beta} = -d^2\bar{u}/dy^2$, (6.46) becomes the so-called Rayleigh equation, which is the most basic one (for a shear instability) with a boundary condition:

$$\tilde{v}(y_1) = \tilde{v}(y_2) = 0 \quad (6.48)$$

in the hydrodynamic instability theor. Namely, we may solve an eigenvalue problem on $\hat{\omega} \equiv \hat{\omega}_r + i\omega_i$, and determine an instability if an eigenvalue satisfying $\omega_i > 0$ (that is, $|\tilde{v}| \rightarrow e^{+\omega_i t} \rightarrow \infty$ for $t \rightarrow \infty$). Another strategy is to obtain an integration theorem as follows: taking $\tilde{v}^* \cdot (1.89) - \tilde{v} \cdot (1.89)^*$:

$$\frac{d}{dy} \Im \left[\tilde{v}^* \frac{d\tilde{v}}{dy} \right] = -\omega_i \frac{k\tilde{\beta}}{|\hat{\omega}|^2} |\tilde{v}|^2,$$

where $()^*$ is the complex conjugate, and $\Im[]$ indicates the imaginary part, we integrate this for $y_1 \leq y \leq y_2$ under the boundary condition (6.48), and obtain

$$\omega_i k \int_{y_1}^{y_2} \tilde{\beta} \frac{|\tilde{v}|^2}{|\hat{\omega}|^2} dy = -\Im \left[\tilde{v}^* \frac{d\tilde{v}}{dy} \right]_{y=y_1}^{y=y_2} = \Im \left[\tilde{v} \frac{d\tilde{v}^*}{dy} \right]_{y=y_1}^{y=y_2} \equiv 0.$$

If an unstable solution ($\omega_i > 0$) exists, the ingration of the left-hand side must be zero, that is, the integrand changes the sign at any point of $y_1 \leq y \leq y_2$. Because $|\tilde{v}|^2/|\hat{\omega}|^2 > 0$, it is requested that $\tilde{\beta} = 0$, that is,

$$\frac{d^2\bar{u}}{dy^2} = \beta \quad \text{somewhere } y_1 < y < y_2, \quad (6.49)$$

which is called the *Kuo's theorem on the barotropic instability* (Kuo, 1949)⁷⁶. Another form of this instability criterion is obtained by substituting $\tilde{v} \equiv \hat{\omega}V$ into (6.46) and (6.47):

$$\hat{\omega} \frac{d^2V}{dy^2} + 2 \frac{d\hat{\omega}}{dy} \frac{dV}{dy} - k^2 \left(\hat{\omega} + \frac{\beta}{k} \right) V = 0, \quad V(y_1) = V(y_2) = 0,$$

taking the difference between this first equation multiplied with $\hat{\omega}V^*$ and its complex conjugate multiplied with $\hat{\omega}^*V$, and integrating the result for $y_1 \leq y \leq y_2$:

$$\bar{u}_{\min} - \frac{\beta}{2k^2} < c_r < \bar{u}_{\max}; \quad (6.50)$$

otherwise taking the sum of them and integrating the result, (in this case ω_i^2 is constant and can be put out of the integral)

$$\left(c_r - \frac{\bar{u}_{\min} + \bar{u}_{\max}}{2} \right)^2 + c_i^2 \leq \left(\frac{\bar{u}_{\min} + \bar{u}_{\max}}{2} \right)^2 + \frac{\beta}{2k^2} (\bar{u}_{\max} - \bar{u}_{\min}), \quad c_i > 0, \quad (6.51)$$

where $c - \bar{u} \equiv \hat{\omega}k$, $c_r - \bar{u} \equiv \hat{\omega}_r k$, $c_r = \omega_r k$, $c_i = \omega_i k$. These are called the Pedlosky's theorem (Pedlosky, 1964, 1979)⁷⁷. In addition, Linzen and Rosenthal (1983) and Lindzen et al. (1983) proposed to apply a concept called *overreflection* to the tropical barotropic instability problems, in which the unstable wave is replaced by a reflection of neutral Rossby wave at the critical point (5.30) with reflectivity > 1 . This gives a unified understanding with the wave-mean flow interaction (Section 5.4): at the critical point, if the flow is stable, the mean flow accelerates by

⁷⁶This is an extension of the so-called Rayleigh's inflection point theorem in the fluid dynamics with $\beta = 0$: if the flow is unstable, the velocity profile must have an inflection point $d^2\bar{u}/dy^2 = 0$ inside the domain.

⁷⁷(6.50) and (6.51) are respectively extensions for $\beta \neq 0$ of the Rayleigh's theorem (an unstable wave must have a critical point (5.30) in the domain) and the Howard's semicircle theorem (the unstable eigenvalues are in a semicircle on the real-axis domain in the Gauss' complex plane; Howard, 1961) obtained originally for $\beta = 0$.

absorbing the waves; whereas if unstable the waves amplify by extracting energy from the mean flow. For further details of the instability problems see dynamics textbooks (e.g., Chapter VII of Charney, 1973; Pedlosky, 1979; Lindzen, 1980; Holton, 1992).

After the approach by barotropic instability did not succeed, the neutral and forced wave theories mentioned in Chapter 5 were developed. The equatorial zone within the deformation radius (4.21) is a “waveguide” (Gill, 1982) for the equatorial waves constituting the MJO. As mentioned in Section 4.1, if the Earth was an “aqua-planet” without any lands, there would be basically zonal structures (right-hand side panel of Fig. 4.7), and the ITCZ near the equator is not homogeneous but involves the MJO/ISVs. In other words a steady zonally-elongated limit or a zonal/seasonal average ISVs become the Hadley circulations (Gill, 1980; Kosaka and Matsuda, 2005).

Those waves are also favorable for the CISK and WISHE mechanisms mentioned in the previous section, which are considered more plausible also for the ISVs. In particular the wave-CISK mechanism (Y. Hayashi, 1970; Lindzen, 1974), which is not assuming the Ekman pumping, is regarded as playing the major role to generate the ISVs such as the MJO, after the pioneering successful numerical experiment of “aqua planet” by Y.-Y. Hayashi and Sumi (1984), which also showed that the ISVs/MJO are the major features over the equatorial atmosphere-ocean system (without land or over the actual open ocean), replacing the steady homogeneous ITCZ imaged since Hadley. When we include the localized heating Q' and substitute the Ooyama’s cumulus parameterization (6.23) and the equivalent depth (5.12), the thermodynamic equation (5.7) for equatorial waves may be rewritten as

$$\frac{\overline{D}\phi'}{Dt} + gh \left(\frac{\partial u'}{\partial x} + \frac{\partial v'}{\partial y} \right) \approx \eta' \left(\frac{\partial u'}{\partial x} + \frac{\partial v'}{\partial y} \right), \quad \eta' > 0. \quad (6.52)$$

From (5.19) gh is square of the phase velocity $\hat{\omega}/k$ (relative to the media moving by the mean flow) of the equatorial Kelvin wave (and gravity waves with $f = 0$) free from any forcing. If the heating exists and is sufficiently strong ($\eta' > gh$), we have $\hat{\omega}^2 < 0$ and expect that any unstable modes ($\hat{\omega} = i\omega_i$, $\omega_i > 0$) exist (Chang and Lim, 1988). Numaguti and Hayashi (1991) examined the aqua-planet model results as a Kelvin wave-CISK, and showed that the results are quite sensitive to the cumulus parameterization scheme. The MJO is noted also as a trigger (or miniature) of the interannual variations such as ENSO (Lau et al., 1989; Lau and Peng, 1990) and IOD. On the other hand, the WISHE mechanism (Emanuel, 1987; Neelin et al., 1987) is expected to work in case of an easterly wave-like situation: wind speed, evaporation and latent heating are stronger in the eastern side (where perturbed wind is also easterly) of a convective updraft area than in the western side. This differential latent heating may intensify the eastward propagating (Kelvin or inertio-gravity) wave with the phase structure that the eastern side is warmer than the western side.

These semi-theoretical approaches, however, are still only qualitatively successful, and have not yet explained the actual dominant time and space scales (zonal wavenumbers and phase velocity of 1–3 and ~ 5 m/s). The too sensitive dependence upon the cumulus parameterization scheme (Numaguti and Hayashi, 1991) has not yet been settled. On the other hand a cloud-resolving model (Miura et al., 2007; Nasuno et al., 2009; Liu et al., 2009) show successful simulation results for some MJO events. Numerical experiments using this model (Takasuka et al., 2015) confirm that MJO/ISVs on an aqua planet are substantially modified if a land such as the IMC blocks the “waveguide” completely. However, a completely satisfactory theory for the MJO/ISVs has not yet been established, so that their prediction is still not good (Waliser, 2012). For further details see several overview articles (Madden and Julian,

1994; Lau and Waliser, 2005; Zhang, 2005, 2013; Yoneyama et al., 2008, 2013).

Zhang (2013) mentioned that the MJO is “bridging weather and climate”. In the tropical marine atmosphere and probably also in the extratropics (including the predictability reason) it would be true. However, in the tropical land the annual cycle (which is basic in the extratropical climatology) is only the second component, but the diurnal cycle is the first. In this meaning the ISVs including MJO in the tropics are like the interannual variations. Of course at least the atmosphere is borderless in space and time, and we need to establish a seamless theoretical meteorology and climatology connecting the tropical marine, tropical land and extratropical atmospheres. Probably the MJO/ISVs over the ocean and the diurnal cycle over lands are both important and collaborating to maintain the energy and water cycles in the Earth’s climate system.

Exercise 6

- (1) Now $T = 20\text{C}$ and $RH = 80\%$. How cold does it become to make cloud or rain?
- (2) At sea level $T=20\text{C}$ and $RH=80\%$. How high is the cloud bottom if it exists?
- (3) What is necessary to realize the cloud bottom as estimated in (2) ?
- (4) If a cloud is generated by 1 km^3 saturated air with $T=20\text{C}$, $p=1000 \text{ hPa}$ and $\rho=1 \text{ kg/m}^3$ and disappears after making rainfall over an area of 1 km^2 , how heavy rain falls?

Answers:

- (1) Roughly in a phase diagram (exactly by solving 2nd eq. of (7)), $e = e_s(T=20\text{C}) \times 0.8 \approx 23 \text{ hPa} \times 0.8 \approx 18 \text{ hPa}$, which is $\approx e_s(T=16\text{C})$, the dew point temperature). Thus, if T cools down to 16C , it may be cloudy or rainy.
- (2) From (1) the cloud bottom (or lifting condensation level=LCL) must be $T=16\text{C}$. Using “dry” lapse rate Γ below the cloud bottom, the bottom is $(20\text{C}-16\text{C})/\Gamma \approx 400 \text{ m}$ height.
- (3) In general a T -profile (as observed by rawinsonde) is slower than Γ , and LCL is warmer than the dew point. Clouds are not generated by air staying at LCL, but by air lifted from the ground (for example by a mountain slope, or by convection forced by hot ground).
- (4) The cloud involves water of $1 \text{ kg/m}^3 \times 10^9 \text{ m}^3 \times 23 \text{ hPa}/1000 \text{ hPa} = 2.3 \times 10^7 \text{ kg}$. Using the density of water 10^3 kg/m^3 , the rainfall amount is $2.3 \times 10^7 \text{ kg}/(10^3 \text{ kg/m}^3)/(10^6 \text{ m}^2) = 2.3 \times 10^{-2} \text{ m} = 23 \text{ mm}$.